Monthly Notices
of the
ROYAL ASTRONOMICAL SOCIETY

MNRAS **495,** 3409–3430 (2020)
Advance Access publication 2020 May 18

doi:10.1093/mnras/staa1345

An ALMA survey of the brightest sub-millimetre sources in the SCUBA-2–COSMOS field

J. M. Simpson,[1,2,3] Ian Smail ,[1]★ U. Dudzevičiūtė ,[1] Y. Matsuda,[3,4] B.-C. Hsieh,[2] W.-H. Wang,[2] A. M. Swinbank ,[1] S. M. Stach,[1] Fang Xia An,[5] J. E. Birkin,[1] Y. Ao,[6,7] A. J. Bunker,[8] S. C. Chapman,[9,10,11] Chian-Chou Chen ,[2] K. E. K. Coppin,[12] S. Ikarashi,[1] R. J. Ivison ,[13] I. Mitsuhashi,[3,14] T. Saito,[15] H. Umehata,[16,14] R. Wang[17] and Y. Zhao [18]

Affiliations are listed at the end of the paper

Accepted 2020 May 7. Received 2020 April 16; in original form 2020 March 11

ABSTRACT

We present an ALMA study of the ∼180 brightest sources in the SCUBA-2 850-μm map of the COSMOS field from the S2COSMOS survey, as a pilot study for AS2COSMOS – a full survey of the ∼1000 sources in this field. In this pilot study, we have obtained 870-μm continuum maps of an essentially complete sample of the brightest 182 sub-millimetre sources ($S_{850\,\mu m} > 6.2$ mJy) in COSMOS. Our ALMA maps detect 260 sub-millimetre galaxies (SMGs) spanning a range in flux density of $S_{870\,\mu m} = 0.7$–19.2 mJy. We detect more than one SMG counterpart in 34 ± 2 per cent of sub-millimetre sources, increasing to 53 ± 8 per cent for SCUBA-2 sources brighter than $S_{850\,\mu m} > 12$ mJy. We estimate that approximately one-third of these SMG–SMG pairs are physically associated (with a higher rate for the brighter secondary SMGs, $S_{870\,\mu m} \gtrsim 3$ mJy), and illustrate this with the serendipitous detection of bright [C II] 157.74-μm line emission in two SMGs, AS2COS 0001.1 and 0001.2 at $z = 4.63$, associated with the highest significance single-dish source. Using our source catalogue, we construct the interferometric 870-μm number counts at $S_{870\,\mu m} > 6.2$ mJy. We use the extensive archival data of this field to construct the multiwavelength spectral energy distribution of each AS2COSMOS SMG, and subsequently model this emission with MAGPHYS to estimate their photometric redshifts. We find a median photometric redshift for the $S_{870\,\mu m} > 6.2$ mJy AS2COSMOS sample of $z = 2.87 \pm 0.08$, and clear evidence for an increase in the median redshift with 870-μm flux density suggesting strong evolution in the bright end of the 870-μm luminosity function.

Key words: galaxies: evolution – galaxies: formation – galaxies: high-redshift – sub-millimetre: galaxies.

1 INTRODUCTION

The brightest high-redshift sources detected in sub-millimetre surveys with single-dish telescopes ($S_{870\,\mu m} \gtrsim 10$ mJy) have far-infrared luminosities of $L_{IR} \gtrsim 10^{13}$ L$_\odot$, which imply star formation rates (SFRs) of $\gtrsim 10^3$ M$_\odot$ yr^{-1} (Barger et al. 2014; Dudzevičiūtė et al. 2020) and classify these systems as HyLIRGs (Hyper-luminous InfraRed Galaxies; Rowan-Robinson 2000; Rowan-Robinson & Wang 2010). The immense SFRs implied for these systems mean that their gas supplies should be rapidly exhausted: ≲100 Myr for a typical sub-millimetre galaxy (SMG) gas mass of ∼10^{11} M$_\odot$ (e.g. Bothwell et al. 2013; Birkin et al., in preparation), and even faster if significant amounts of gas are expelled from the systems by outflows. This is ∼5 per cent of the length of the era where the activity in the SMG population peaks: $z \sim 1.8$–3.4 (e.g. Chapman et al. 2005; Simpson et al. 2014; Dudzevičiūtė et al. 2020), underlining the potentially short-lived nature and high duty cycle of these extreme events.

Although short-lived, HyLIRG SMGs may represent the most significant individual star-forming events in the Universe, potentially forming an ∼L^* worth of stars in a few 10's of Myr (e.g. Ivison et al. 2010, 2013). Indeed, the intensity of this starburst activity would likely out-radiate all other processes (such as emission from AGNs) that can confuse the interpretation of systems with less extreme SFRs. Moreover, while extreme, the star formation

★ E-mail: ian.smail@durham.ac.uk

processes in these SMGs may be similar to those occurring in a less intense manner in the more numerous bulk of the SMG population, and so their study can aid our understanding of the whole population.

The number density and physical properties of HyLIRG SMGs, which lie on the rapidly diminishing tail of high-luminosity sources, are frequently the most challenging for galaxy formation models to reproduce (e.g. Chakrabarti et al. 2008; Swinbank et al. 2008; Davé et al. 2010; McAlpine et al. 2019), and they can thus provide strong constraints on these models. However, the reality of many of these extremely luminous SMGs detected in wide-area, but low-resolution, single-dish surveys has been called into question. Strong lensing is clearly responsible for the apparent luminosities of the very brightest sub-millimetre sources, $S_{870\,\mu m} \gg 10$–100 mJy (e.g. Swinbank et al. 2010b; Ikarashi et al. 2011; Harrington et al. 2016). However, at somewhat fainter fluxes another concern has arisen from high-resolution interferometric studies, first with SMA and subsequently from ALMA, which suggest that a moderate proportion of bright single-dish sources comprise blends of fainter sources (e.g. Wang et al. 2007, 2011; Younger et al. 2009; Karim et al. 2013; Simpson et al. 2015a; Stach et al. 2018). The low resolution of current single-dish sub-millimetre surveys thus appears to frequently blend several SMGs within a beam to produce a single brighter source, changing the shape of the number counts, most critically by producing a false tail of bright sources, which can also be further boosted by gravitationally lensed sources. This then complicates the use of these single-dish sub-millimetre counts as an observational constraint on galaxy formation and evolution models (Cowley et al. 2015).

We have undertaken an ALMA continuum survey of bright sub-millimetre sources to investigate these issues, with the goals of determining the intrinsic form of the bright sub-millimetre counts, better quantifying the influence of blending on single-dish sources, and identifying a sample of intrinsically luminous SMGs to study their physical properties (including the role of any nearby companions in triggering their intense activity). This pilot study is based on the brightest sub-millimetre sources selected from the SCUBA-2 850-μm survey of the COSMOS field undertaken by the S2COSMOS project (An et al. 2019; Simpson et al. 2019). This ALMA–S2COSMOS (AS2COSMOS) pilot survey represents a systematic programme to obtain, or collate, sub-arcsecond-resolution, sub-millimetre follow-up observations of a complete sample of 850-μm-luminous, single-dish-selected sources in this well-studied field. We will discuss the multiwavelength properties of these sources in Ikarashi et al. (in preparation) and a sample of serendipitously detected line emitters from our ALMA data cubes in Mitsuhashi et al. (2020). Our survey is also complemented by the analysis of all ALMA archival observations of sources within COSMOS that has been undertaken by Liu, Schinnerer, and co-workers (Liu et al. 2019). That study includes a larger sample of sources, but it has a more heterogeneous selection (and also mix of ALMA data products) than our study.

The structure of the paper is as follows: In Section 2, we discuss our sample selection, the ALMA observations, and our data reduction, including the construction of our source catalogue and a comparison between the ALMA and SCUBA-2 detections. We also review the available multiwavelength supporting data. In Section 3, we describe the number counts of sub-millimetre sources we derive, estimate the prevalence of multiple SMGs within SCUBA-2 sources in our survey, including a particularly bright example where we have serendipitous confirmation that the two components are associated, and discuss the photometric redshift distribution and trends with sub-millimetre flux in our sample. Finally, in Section 4 we give our conclusions. We adopt a ΛCDM cosmology with $H_0 = 70\,\mathrm{km\,s^{-1}\,Mpc^{-1}}$, $\Omega_\Lambda = 0.7$, and $\Omega_m = 0.3$ and, unless otherwise stated, error estimates are from a bootstrap analysis. All magnitudes quoted in our work are in the AB photometric system and we assume a Chabrier (2003) initial stellar mass function throughout.

2 OBSERVATIONS, REDUCTION, AND ANALYSIS

2.1 Sample selection

The parent sample for our work is selected from a sensitive 850-μm map of the COSMOS field obtained with SCUBA-2 (Holland et al. 2013) at the James Clerk Maxwell Telescope (JCMT). This SCUBA-2–COSMOS (S2COSMOS; Simpson et al. 2019) survey is comprised of two tiers: a MAIN region that reaches a median sensitivity of $1.2\,\mathrm{mJy\,beam^{-1}}$ over the $1.6\,\mathrm{deg^2}$ *Hubble Space Telescope*/Advanced Camera for Surveys footprint (Koekemoer et al. 2007) and a SUPPLEMENTARY region that provides an additional $1\,\mathrm{deg^2}$ of coverage at a median sensitivity of $1.7\,\mathrm{mJy\,beam^{-1}}$. In this paper, we only consider the 1020 single-dish-identified sources ($S_{850\,\mu m} = 2$–20 mJy) that were detected at the $>4\sigma$ significance level in the S2COSMOS MAIN survey.

For the ALMA Cycle-4 proposal deadline (2016 April), we employed a preliminary version of the S2COSMOS MAIN source catalogue to identify 160 targets for a pilot study into the properties of the most luminous 850-μm sources ($S_{850\,\mu m} \gtrsim 8$ mJy) in the COSMOS field. Due to a delay in the completion of our ALMA project (see Section 2.2) and ongoing improvements to the sensitivity of the S2COSMOS map, we subsequently adjusted our initial sample selection while retaining the aim of obtaining a flux-limited sample of 850-μm-luminous sources. As such, in our ALMA Cycle-4 programme, we obtained Band 7 imaging for 160 S2COSMOS sources (Fig. 1), of which 158 have deboosted/deblended flux densities $S_{850\,\mu m} > 6.2$ mJy. We note that two SCUBA-2 sources that were observed in the Cycle-4 project scattered to $S_{850\,\mu m} < 6.2$ mJy in the final S2COSMOS source catalogue ($S_{850\,\mu m} = 5.5 \pm 1.2$ and 6.1 ± 1.6 mJy).

The final S2COSMOS MAIN source catalogue contains 183 sources with deboosted/deblended 850-μm flux densities > 6.2 mJy (Simpson et al. 2019). These sources are detected in the S2COSMOS map at a significance ranging from 5.4σ to 28σ and, as such, we expect the sample to have a false detection rate $\ll 1$ per cent (Simpson et al. 2019). In our Cycle-4 programme, we obtained sensitive 870-μm imaging of 158 of these sources and we subsequently identified suitable archival ALMA Band 7 imaging (see Section 2.2) for a further 24. Combining our Cycle-4 observations with the existing archival data means that our AS2COSMOS pilot study is 99.5 per cent (182/183) complete for single-dish-identified sources with deboosted/deblended flux densities of $S_{850\,\mu m} > 6.2\,\mathrm{mJy\,beam^{-1}}$ (see Fig. 2), over a survey area of $1.6\,\mathrm{deg^2}$. Note that we present our ALMA Cycle-4 maps of two S2COSMOS sources with flux densities < 6.2 mJy but do not include them in our analysis, where relevant (e.g. source counts).

Finally, we note that there have been a number of prior studies into the properties of far-infrared-luminous sources in the COSMOS field (e.g. Younger et al. 2007, 2009; Smolčić et al. 2012; Brisbin et al. 2017; Hill et al. 2018; Liu et al. 2019). A literature search identifies that 45 of the 160 targets in our Cycle-4 ALMA

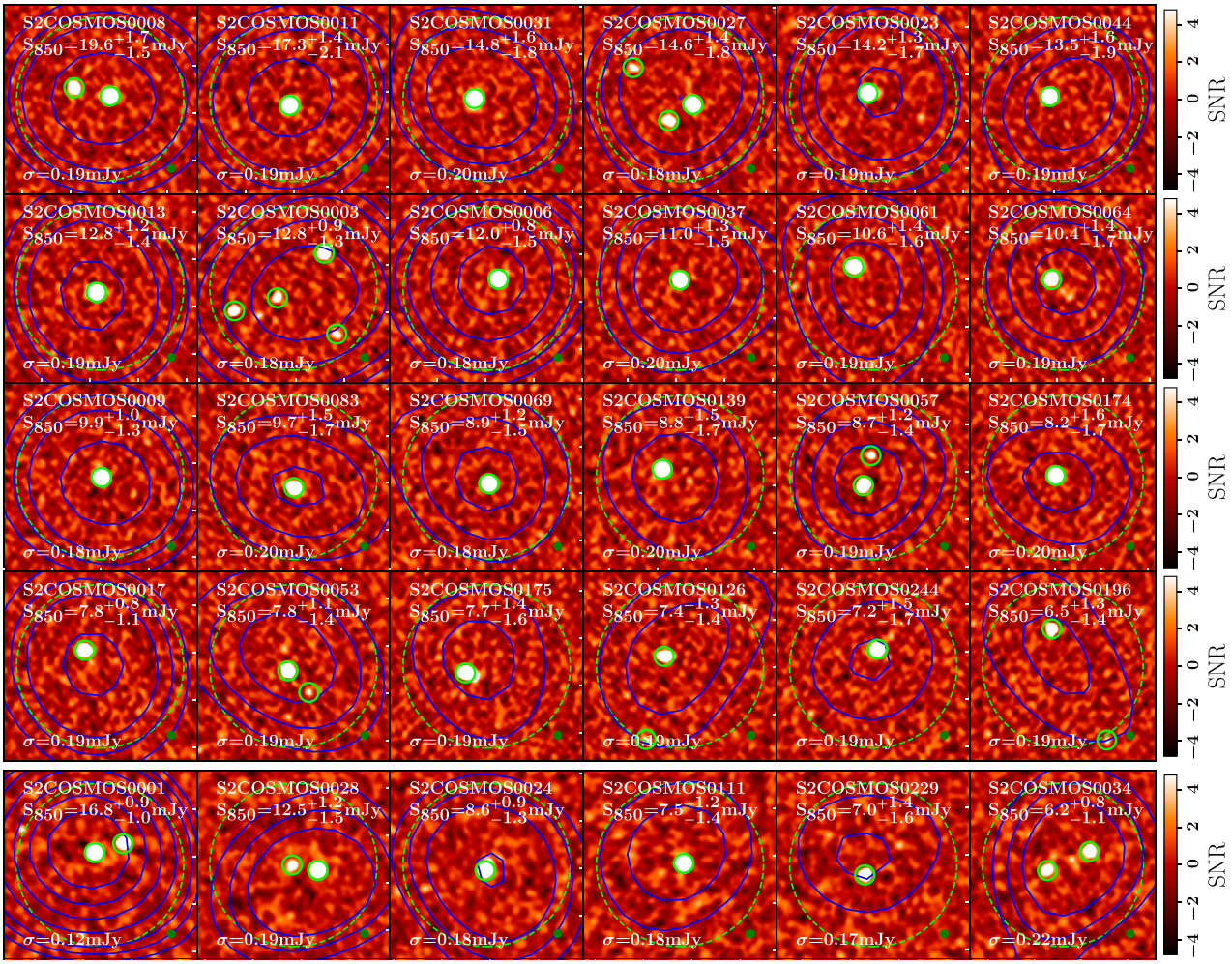

Figure 1. 30 example ALMA 870-μm continuum maps, displayed as signal-to-noise ratio maps from $\pm 5\sigma$, from our pilot survey of the 182 brightest SCUBA-2-identified sources in the COSMOS field. The top four rows were selected at random from our 160 Cycle 4 ALMA targets in bins of single-dish flux density (in descending flux from the top row: $S_{850\,\mu m} = 13$–20, 10–13, 8–10, and 6–8 mJy). Our AS2COSMOS pilot survey includes 24 archival ALMA maps and we show a randomly chosen subset of these in the final row to highlight that they have a comparable quality to our Cycle 4 data. We detect 260 SMGs (circled) at $> 4.8\sigma$ across the 182 ALMA 870-μm maps, with flux densities of 0.7–19.2 mJy. The presence of multiple continuum counterparts in a fraction of the maps is clear (e.g. S2COSMOS 0003; see Section 3.3). Solid contours represent SCUBA-2 emission at 4σ, 6σ, 8σ, 12σ, 16σ, 20σ, and 24σ. The panels are 20 × 20 arcsec (160 × 160 kpc at $z \sim 2.5$), the dashed circle represents the 17.3 arcsec primary beam of ALMA at 870 μm, and we show the synthesized beam in the bottom right of each map, as well as a colour bar indicating the signal-to-noise scaling on the right of each row.

programme have sub-/millimetre interferometric observations that were typically undertaken with ALMA and/or PdBI at 1.2–1.3 mm (Smolčić et al. 2012; Brisbin et al. 2017), or at ∼870 μm with the SMA (e.g. Younger et al. 2009; Hill et al. 2018). To ensure that AS2COSMOS represents a homogenous study of the 850-μm-luminous population, we retained these 45 targets in our ALMA Cycle-4 programme: Follow-up observations conducted at a different wavelength to that of the initial sample selection can introduce dust-temperature biases that are challenging to quantify, while the depth of the SMA maps ($\sigma \sim 1$–2 mJy beam^{-1}) means that the observations are relatively incomplete to sources that lie close to, or below, the flux threshold of our single-dish selection ($S_{850\,\mu m} > 6.2$ mJy beam^{-1}). We cross-match our pilot AS2COSMOS sample with these pre-existing catalogues of sub-/millimetre interferometrically identified SMGs and provide any alternative identifications in Table 1.

2.2 ALMA data reduction

Between 2018 May 15 and 21, we obtained ALMA Band 7 observations of 160 S2COSMOS sources, under project ID: 2016.1.00463.S (PI: Y. Matsuda). Observations were undertaken with a standard correlator set-up for continuum, with four basebands providing 7.5-GHz bandwidth at a central frequency of 343 GHz (870 μm). For each target, the ALMA pointing centre was fixed to the S2COSMOS source position and, at our observing frequency, the ALMA primary beam (FWHM = 17.3 arcsec) is well-matched to the SCUBA-2/JCMT beam (effective FWHM = 14.6 arcsec; Dempsey et al. 2013).

Our 160 targets were observed in two 'blocks' containing 79 and 81 sources, respectively. Each 'block' was observed twice, resulting in a total of four measurement sets. Observations of each 'block' were conducted with 46 and 48 12-m antennae, respectively, on baselines ranging from 15 to 310 m (median baseline length of

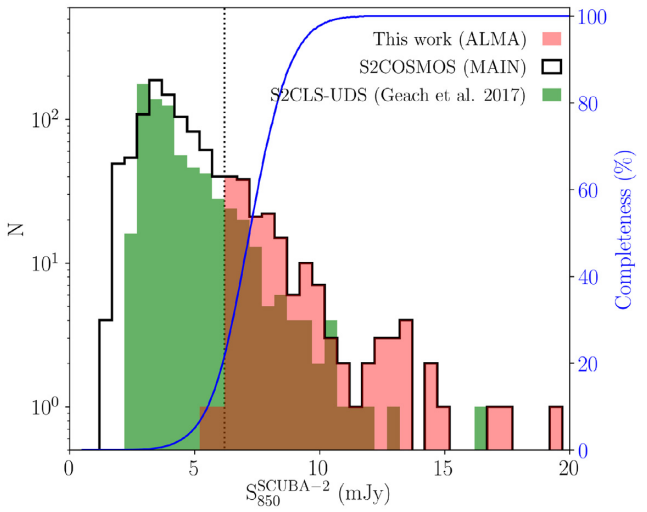

Figure 2. The 850-μm flux density distribution of the 182 single-dish-identified sources that comprise our ALMA–S2COSMOS pilot study, compared to the parent distribution of S2COSMOS MAIN sources. The AS2COSMOS pilot survey is effectively complete for S2COSMOS sources brighter than 6.2 mJy (182/183; dotted line). For comparison, we show the flux distribution for the S2CLS-UDS sample of SCUBA-2-identified sources (Geach et al. 2017), the parent sample for a similar ALMA follow-up study (AS2UDS; Stach et al. 2019), to demonstrate that AS2COSMOS has roughly twice the source numbers at $S_{850\,\mu m} > 6.2$ mJy, relative to a comparable, degree-scale survey. The solid curve represents the effective completeness of the AS2COSMOS pilot survey after accounting for incompleteness in AS2COSMOS and S2COSMOS studies, as well as the effect of a fixed selection at $S_{850\,\mu m} > 6.2$ mJy on the S2COSMOS catalogue. AS2COSMOS is estimated to be 22, 50, and 90 per cent complete to sources at $S_{850\,\mu m} = 6.2$, 7.2, and 8.9 mJy, respectively, across a survey area of 1.6 deg^2.

90 m). Calibration observations were obtained for each measurement set and the same set of calibrators was used throughout. Each measurement set was calibrated in CASA v 5.1.1 using the standard reduction pipeline. Phase calibration was conducted using J 0948+0022, which was observed periodically on a 7-min cycle, while the absolute flux scale and bandpass were set on J 1058+0133. We visually inspected the pipeline calibrated data and used the CASA/CONCAT task to combine the observations of each target into a single measurement set for imaging.

We also include data on a further 24 S2COSMOS sources that were observed in seven publicly available, archival ALMA projects.[1] To ensure homogeneity across the AS2COSMOS sample, the archival observations were selected on the following criteria: They must have: a pointing centre <3 arcsec from the SCUBA-2 source position (16–84th percentile range from 0.6 to 2.1 arcsec); be obtained at an observing frequency of 343 GHz, and achieve a 1σ sensitivity of $\lesssim$0.2 mJy beam^{-1}, after applying a taper to broadly match the resolution of our Cycle-4 maps (FWHM $\sim$ 0.8 arcsec). For each of the archival projects considered here, we retrieved the relevant measurement sets from the ALMA archive and reran the data reduction pipeline to fully calibrate the data. Each of the calibrated data sets was visually inspected and any minor issues were corrected (e.g. additional channel flagging).

Imaging the *uv*-data for the AS2COSMOS sources was conducted using CASA v 5.1.1, with the new and archival data treated identically. To image each of our science targets, we first Fourier transform the *uv*-data to obtain a dirty image, adopting Briggs weighting (robust parameter = 0.5). Small variations in the resolution of the AS2COSMOS maps were accounted for on a map-by-map basis by identifying and applying a two-dimensional Gaussian taper in the *uv*-plane. The appropriate *uv*-taper was chosen such that the synthesized beam of the resulting map has an FWHM $\sim$ 0.8 arcsec that is well matched to the resolution of the 'new' 160 AS2COSMOS observations presented here. We note that for three of the AS2COSMOS targets we cannot construct a *uv*-taper that achieves our target resolution. The *uv*-coverage for the observations of S2COSMOS 0038 and 0111 yields a synthesized beam of 0.95 × 0.80 arcsec, while for S2COSMOS 0188 we found that further tapering beyond 0.50 × 0.47 arcsec resulted in a rapid degradation in sensitivity ($\gg$0.2 mJy beam^{-1}). Overall, the AS2COSMOS pilot sample has a median synthesized beam of 0.80 × 0.79 arcsec with a variation of <0.02 arcsec across 181 out of 182 maps (see Table 1).

To clean each of the AS2COSMOS dirty images, we use the TCLEAN task within CASA and a two-step procedure. First, the sensitivity of the dirty map was estimated using an iterative, sigma-clipping technique ($\pm 4\sigma$). Any sources detected at $\geq 6\sigma$ in the dirty image were masked using the TCLEAN automasking routine, and the masked regions cleaned to 2σ. Note that we enforce that any identified sources are detected at >4 × the expected peak side-lobe level. After the initial clean process has completed, we reassess the sensitivity of the map, excluding any masked regions, and perform a second clean. For the second clean process, we identify any sources detected at $\geq 4.25\sigma$ and clean these to $1\sigma_{870\,\mu m}$ using the same automasking procedure. The resulting maps have a range of $1\sigma_{870\,\mu m}$ depths from 0.11 to 0.22 mJy beam^{-1} (10–90th percentile $\sigma_{870\,\mu m}$ = 0.18–0.20 mJy beam^{-1}) and a median sensitivity of $\sigma_{870\,\mu m} = 0.19$ mJy beam^{-1} (see Table 1). All maps have a pixel scale of 0.1 arcsec and a size of 25.6 arcsec × 25.6 arcsec. Representative examples of these data are shown in Fig. 1.

2.2.1 *Source extraction*

To construct a source catalogue for our AS2COSMOS pilot survey, we first use SEXTRACTOR (Bertin & Arnouts 1996) to identify any >2σ 'peaks' in the non-primary-beam-corrected ALMA maps (Fig. 1). At the position of each potential source, we measure both the peak flux density and the integrated flux density, using an aperture with a diameter of 1.5 × the major axis (FWHM) of the synthesized beam. The associated uncertainty on the integrated fluxes is calculated by placing 100 apertures at random on the source-subtracted ALMA maps and taking the standard deviation of the resulting aperture flux densities.

We expect that our preliminary catalogue of >2σ 'peaks' is subject to strong contamination from false detections. To estimate the required significance cut for a robust catalogue of sources, we invert the ALMA maps and repeat our source extraction procedure. Within the ALMA primary beam, we find that the number of false detections falls to zero at a peak or aperture significance of >4.8σ and >4.9σ, respectively, and we adopt these criteria here. Applying these selection limits to our preliminary catalogue, we obtain a robust sample of 254 SMGs, with each of the 182 ALMA maps containing a minimum of one SMG.

A visual inspection of the AS2COSMOS maps indicates the presence of potentially bright sources located marginally outside the ALMA primary beam. Extending our analysis to the entire

[1]Project IDs: 2013.1.00034.S, 2013.1.01292.S, 2015.1.00568.S, 2015.1.01074.S, 2015.1.00137.S, 2016.1.00478.S, and 2016.1.01604.S.

Table 1. AS2COSMOS source catalogue.

ID	R.A. (J2000)	Dec. (J2000)	$S_{\rm SCUBA\text{-}2}$ (mJy)	Map rms[a] (mJy beam^{-1})	Beam (arcsec)	SNR	$S^{b}_{\rm ALMA}$ (mJy)	Other ID[c]
AS2COS0001.1	10:00:08.04	+02:26:12.3	$16.8^{+0.9}_{-1.0}$	0.12	0.80 × 0.77	104.5	$13.5^{+0.3}_{-0.3}$	AzTEC2, COSLA4, AzTECC3a
AS2COS0001.2	10:00:07.84	+02:26:13.2	$16.8^{+0.9}_{-1.0}$	0.12	0.80 × 0.77	27.8	$3.6^{+0.2}_{-0.2}$	AzTECC3c
AS2COS0002.1	10:00:15.61	+02:15:49.0	$13.3^{+0.7}_{-1.4}$	0.12	0.80 × 0.76	85.7	$13.2^{+0.3}_{-0.2}$	MM1, COSLA1, AzTECC7
AS2COS0003.1	10:00:56.95	+02:20:17.3	$12.8^{+0.9}_{-1.3}$	0.18	0.81 × 0.79	30.5	$7.5^{+0.3}_{-0.3}$	HCOSMOS02.0, 131077, AzTECC6a
AS2COS0003.2	10:00:57.57	+02:20:11.2	$12.8^{+0.9}_{-1.3}$	0.18	0.81 × 0.79	15.0	$5.1^{+0.4}_{-0.4}$	,HCOSMOS02.1, 130891, AzTECC6b
AS2COS0003.3	10:00:57.27	+02:20:12.6	$12.8^{+0.9}_{-1.3}$	0.18	0.81 × 0.79	10.1	$2.2^{+0.3}_{-0.3}$	HCOSMOS02.4, 130933
AS2COS0003.4	10:00:56.86	+02:20:08.8	$12.8^{+0.9}_{-1.3}$	0.18	0.81 × 0.79	6.6	$2.5^{+0.5}_{-0.5}$	HCOSMOS02.2, 130949
AS2COS0004.1	10:00:19.75	+02:32:04.2	$13.2^{+0.9}_{-1.1}$	0.22	0.81 × 0.79	26.3	$10.8^{+0.6}_{-0.5}$	AzTEC5, AzTECC42
AS2COS0005.1	10:00:23.97	+02:17:50.1	$10.3^{+0.8}_{-1.0}$	0.19	0.81 × 0.79	29.9	$8.4^{+0.4}_{-0.3}$	–
AS2COS0005.2	10:00:24.03	+02:17:49.4	$10.3^{+0.8}_{-1.0}$	0.19	0.81 × 0.79	7.5	$2.1^{+0.4}_{-0.3}$	–
...	...	...	...	...	...	...	...	...

Note. The AS2COSMOS source catalogue, showing the sources that are detected in our ALMA maps of the highest significance SCUBA-2 detections across the 1.6-deg^2 S2COSMOS MAIN survey region. The full catalogue is available in the online journal. [a] 1σ sensitivity of the non-primary-beam-corrected ALMA map. [b] Total flux density, corrected for the ALMA primary beam response. [c] Cross-matched identifications for AS2COSMOS SMGs that have been detected in prior sub-/mm interferometric observations (see Younger et al. 2007, 2009; Aravena et al. 2010; Smolčić et al. 2012; Bussmann et al. 2015; Wang et al. 2016; Brisbin et al. 2017; Hill et al. 2018).

imaged area, we find that the false-detection rate falls to zero at a slightly higher peak significance of $>5.1\sigma$, relative to the primary beam area, reflecting the lower data quality in outer parts of each map. We identify six SMGs[2] that are located 8.9–11.5 arcsec from the phase centre of the relevant map (i.e. outside the primary beam) at a peak detection significance of 5.1σ–10.3σ. These sources are included in our source catalogue and we note that five of the six have a clear counterpart in the available IRAC/3.6-μm imaging of the COSMOS field.

Overall, our pilot survey of 182 S2COSMOS sources yields a sample of 260 AS2COSMOS SMGs with a median detection significance of 24σ (10–90th percentile range 6.5σ–46σ). The brightest SMG in each ALMA pointing is typically located close to the phase centre of the map, with a median offset to the parent SCUBA-2 source of 0.46 ± 0.13 arcsec. Moreover, the median offset in R.A. and Dec. between the positions is 0.29 ± 0.10 and 0.10 ± 0.13 arcsec, respectively, indicating a good overall level of astrometric agreement between the surveys. In Table 1, we provide the basic observable properties for each AS2COSMOS source as well as cross-matched identifications for the 69 AS2COSMOS SMGs that have been detected at ∼arcsec resolution in prior sub-/millimetre interferometric observations.

2.3 Flux estimation

We determine the total flux density of each AS2COSMOS SMG by modelling their 870-μm emission in the *uv*-plane. High-resolution ALMA imaging of comparable samples of single-dish-identified SMGs indicates that the observed 870-μm emission can be well described by a Sersic profile (e.g. Hodge et al. 2016; Gullberg et al. 2019), and we adopt that model here. During the fitting procedure we leave five parameters of our model free to vary (R.A., Dec., flux density, half-light radius, and axial ratio) but, given the modest resolution of our ALMA data (FWHM ∼ 0.8 arcsec), we fix the Sersic index at $n = 1$, the median best-fitting value for 154 of the brighter AS2UDS SMGs observed at 0.15-arcsec resolution in ALMA Band 7 (Gullberg et al. 2019).

Calibrated visibilities for each ALMA target were extracted using CASA and modelled using a custom written code utilizing three publically available packages. First, we use PROFIT (Robotham et al. 2017) to construct a pixelated model for all detected SMGs that are detected in a given AS2COSMOS map. This model image is then Fourier transformed into the *uv*-plane using GALARIO (Tazzari, Beaujean & Testi 2018), which yields model visibilities based on the *uv*-coverage of the relevant AS2COSMOS map. Finally, we estimate the best-fitting parameters for the input model by minimizing the difference between the observed and model visibilities, using χ^2 minimization and the LMFIT non-linear optimization suite. False minima in χ^2 were mitigated against by repeating the parameter optimization 10 times using randomly selected starting parameter values, with the iteration at the lowest χ^2 value taken as the best-fitting solution.

To estimate the associated uncertainties and characterize any underlying bias on the best-fitting flux densities, we create a Monte Carlo simulation comprising 10^6 simulated ALMA data sets. Each simulated data set is constructed by injecting a single model source into the residual data for a randomly selected AS2COSMOS target. The model source is injected at a random position within a residual map with a Sersic $n = 1$ light profile that is convolved with the appropriate synthesized beam. The axial ratios and half-light radii of the model sources are drawn at random from a uniform distribution between zero and one, and 0.05 and 0.30 arcsec, respectively, with the latter chosen to match the distribution of angular sizes measured for the 154 AS2UDS SMGs from Gullberg et al. (2019). The flux density of each model source is randomly sampled from the parametrized estimate of the sub-/millimetre counts presented by Hatsukade et al. (2018), with a low flux cut-off at $S_{870\,\mu\rm m} = 0.05$ mJy.

We run our source-detection and visibility-modelling procedures on the simulated data and record the best-fitting model parameters for all sources that satisfy our detection criteria. Analysing the results of the simulation, we identify the well-known effect of flux boosting, or Eddington bias (Eddington 1913), on the recovered flux densities of the simulated sources. Flux boosting describes the statistical overestimation of the flux density of a source detected at a low signal-to-noise ratio due to the steep shape of the source counts and the effect of random noise fluctuations. On average, the recovered flux density of a 4.8σ source in our simulation is boosted by 15 per cent, decreasing to a <4 per cent bias at $>10\sigma$. To estimate a statistical correction for flux boosting, we calculate the median ratio between the recovered and input flux densities of the simulated sources as a function of their detection significance. We use the running median to correct the flux densities of the sources in our AS2COSMOS catalogue, based on their detection significance, and

[2] AS2COS 0015.3, 0055.3, 090.2, 0129.3, 0192.2, and 0196.2.

estimate the associated uncertainty on the corrected fluxes from the 1σ scatter in the boosting correction. The corrected flux density and associated error from our *uv*-modelling are adopted as the best estimate for each AS2COSMOS source, and are provided in Table 1.

Next, we consider the recovered flux density of the simulated sources as a function of input half-light radius. We find that the recovered flux density is unbiased for the average source but we do identify a tendency of over/underestimating the flux densities of sources at smaller/larger half-light radii. The maximum bias is estimated to be 4 per cent for sources detected at $<10\sigma$, falling to <1 per cent for sources detected at $>15\sigma$ ($S_{870\,\mu\mathrm{m}} \gtrsim 4.5$ mJy). While we caution that this bias exists for fainter AS2COSMOS source, we stress that our analysis is focused on the bright end of the SMG population ($S_{870\,\mu\mathrm{m}} > 6.2$ mJy), for which any bias is negligible.

Finally, our parametric estimate for the flux density of each AS2COSMOS SMG may be biased if their 870-μm emission is not accurately described by a single Sersic profile. To quantify this effect, we compare the best-fitting model flux density for each SMG to the aperture flux density measured during the source detection process. Before making a comparison, we must first estimate a correction for the fraction of the total emission that falls outside our adopted aperture. We estimate the aperture correction by creating a stacked radial profile of the emission from all 260 AS2COSMOS SMGs, normalized by their flux density in an aperture with a diameter of 1.5 × the beam FWHM (see Section 2.3). The resulting profile converges at a radius of $\gtrsim$1.4 arcsec with a corresponding average aperture correction of 1.44 ± 0.01. Applying this correction to the aperture flux densities of the AS2COSMOS SMGs to derive empirical total fluxes, we find agreement with the results from our Sersic profile fitting at the ± 1.5 per cent level, confirming that our model fitting procedure is robust on average.

2.4 Completeness and flux recovery

Next, we use our Monte Carlo simulations to estimate the completeness level of the AS2COSMOS pilot survey. As expected, the simulations demonstrate that the completeness level of the ALMA maps is strongly dependent on both the angular size and flux density of the input source. If we consider sources with input flux densities $S_{870\,\mu\mathrm{m}} > 6.2$ mJy, i.e. the sample selection for the AS2COSMOS pilot survey, we estimate that our survey is >99.9 per cent complete for sources with half-light radii <1 arcsec (this was derived by extending our analysis in the previous section to a broader range in sizes for the SMGs). Prior observations have suggested that typical SMGs have observed a 870-μm half-light radius of ∼0.1–0.2 arcsec (Ikarashi et al. 2015; Simpson et al. 2015a; Hodge et al. 2016; Gullberg et al. 2019); as such, we consider our catalogue to be complete for SMGs brighter than $S_{870\,\mu\mathrm{m}} = 6.2$ mJy.

We stress that our estimate for the completeness level of the AS2COSMOS pilot does not account for any incompleteness in the parent SCUBA-2 sample. The S2COSMOS MAIN survey is estimated to be 87 per cent complete to sources with flux densities of $S_{870\,\mu\mathrm{m}} = 6.2$ mJy (Simpson et al. 2019), meaning that 87 per cent of sources with this intrinsic flux density are catalogued with fluxes above the S2COSMOS flux limit. However, that does not mean that all sources with *intrinsic* fluxes of $S_{870\,\mu\mathrm{m}} = 6.2$ mJy will appear above the *observed* flux limit of $S_{870\,\mu\mathrm{m}} > 6.2$ mJy that was used to select targets for ALMA follow-up imaging, due to the influence of noise fluctuations in the SCUBA-2 map. Following the procedure detailed in Simpson et al. (2019), we estimate the formal completeness level of the S2COSMOS survey accounting for the sample selection of AS2COSMOS. Accounting for all potential sources of noise and incompleteness, we estimate that the AS2COSMOS observed flux limit of $S_{870} > 6.2$ mJy means that we include 22 and 90 per cent of SMGs with intrinsic flux densities of $S_{870\,\mu\mathrm{m}} = 6.2$ and 9.0 mJy (see Fig. 2), respectively, that are located within a 1.6-deg^2 footprint centred on the COSMOS field. However, we stress that the modest completeness of sources with $S_{870\,\mu\mathrm{m}} = 6.2$ mJy mostly arises from scattering of sources in a narrow flux range around the adopted flux limit.

Next, we assess how much of the flux of the S2COSMOS sources is recovered in the SMGs detected in our ALMA maps. To achieve this, we create a model map for each AS2COSMOS source that contains all ALMA-detected SMGs, which we convolve with an empirical estimate of the SCUBA-2 beam (Simpson et al. 2019). We compare the peak flux density of the convolved maps to the raw *observed* SCUBA-2 flux densities finding a median ratio of the convolved ALMA-to-SCUBA-2 flux density of 0.94 ± 0.01. As expected, the convolved ALMA flux densities are marginally lower than the observed SCUBA-2 fluxes, reflecting that we have not accounted for the effect of flux boosting, or Eddington bias, in the single-dish map.

Deboosting corrections for each SCUBA-2 source are provided by Simpson et al. (2019), but these model-dependent corrections account for both Eddington bias and line-of-sight multiplicity. To isolate the Eddington bias correction, we follow the approach in Simpson et al. (2019) and construct 100 *end-to-end* simulations of the S2COSMOS survey, using our best-fitting parametrization for the sub-millimetre number counts as the input model (see Section 3.1). Sources were extracted from the simulated S2COSMOS images and we recorded the position and flux of all sub-millimetre emitters ($S_{850\,\mu\mathrm{m}} \gtrsim 0.05$ mJy) that were injected within 8.7 arcsec of each of the recovered SCUBA-2 positions. For each simulated SCUBA-2 source, we identified the corresponding set of sub-millimetre emitters and injected these into a randomly chosen residual map from the AS2COSMOS pilot survey at their model position and flux density. Finally, we ran our source extraction procedure on the simulated ALMA maps cataloguing any sources that lie above our threshold for detection and estimating their deboosted flux density.

We can use these simulations to compare the fluxes of the *brightest* component in each ALMA map to the estimated flux for that source from Simpson et al. (2019), which included statistical corrections for both blending and noise boosting. We note that the statistical correction for line-of-sight multiplicity assumes no clustering, although it appears that physically associated SMG–SMG pairs do not dominate in the overall AS2COSMOS sample (see Section 3.3). We find that flux density of the brightest SMG in each ALMA map is, on average, 0.99 ± 0.01 of the flux density of the corrected SCUBA-2 source (see Fig. 3), which shows good agreement between the flux scales of the two surveys. This suggests that with knowledge of the *true form* of the SMG number counts, it is possible to statistically correct for the effects of both multiplicity and boosting in single-dish counts to estimate *on average* the true sub-millimetre brightness of the counterparts. We also note that these simulations not only allow us to test the completeness of our survey, but also assess the contribution of clustering on the presence of multiple SMG counterparts in a single-dish source, as we show in Section 3.3.

In summary, we conclude that the AS2COSMOS SMGs we have catalogued account for the bulk of the emission from the targeted SCUBA-2 sources, although we reiterate that there is a nominal flux calibration uncertainty of ∼5 per cent on both flux scales.

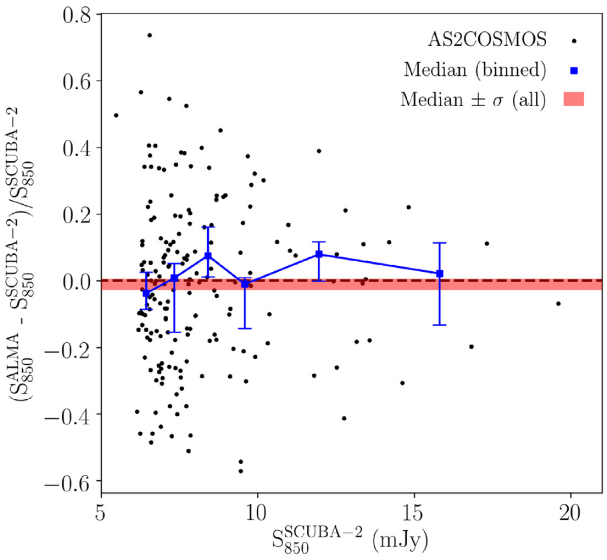

Figure 3. Comparison between the flux density of the brightest component in each AS2COSMOS map and the flux density of the targeted SCUBA-2 source *after statistical correction of the latter for boosting and blending*. Overlaid is the median flux recovery and associated uncertainty for all 182 AS2COSMOS maps (shaded), as well as the running median in bins (≥ 0.5 mJy; solid line) that contain no fewer than 10 sources. We find a statistically insignificant deficit of $-0.01^{+0.01}_{-0.02}$ mJy in the recovered flux density and note that the associated error does not include the expected flux calibration uncertainty of ∼5 per cent for both samples. This demonstrates that the statistical deblending and deboosting corrections applied by Simpson et al. (2019) are, on average, able to recover the correct flux for the brightest ALMA component, although there is considerable uncertainty on the flux of any specific source.

2.5 Archival multiwavelength observations

The COSMOS field has been the target of numerous imaging campaigns at X-ray-to-radio wavelengths, and has one of the deepest sets of multiwavelength data available over a degree-scale area. We make use of this extensive imaging to construct the UV-to-radio spectral energy distribution (SED) of each AS2COSMOS SMG, which we subsequently model to derive their physical properties (e.g. photometric redshifts and far-infrared luminosities) in Ikarashi et al. (in preparation). The following describes the data sets used in our analysis and the methods used to determine the multiwavelength photometry of the AS2COSMOS SMGs. We also use these data in Fig. 4 (see also Fig. A1) to illustrate the appearance of the SMGs in our sample in the observed near-/mid-infrared wavebands.

2.5.1 Optical-to-near-infrared imaging

The COSMOS2015 catalogue (Laigle et al. 2016) includes 27-band, optical-to-near-infrared photometry for near-infrared-selected sources in the COSMOS field. Laigle et al. (2016) homogenize the *u*-to-K_s-band imaging (FWHM ∼ 0.5–1.0 arcsec) to a broadly consistent point spread function (PSF) and identify sources in a stacked $zYJHK_S$ 'detection' image. For each detected source, flux densities are extracted in a 3-arcsec diameter aperture on the PSF-homogenized images and aperture corrected to a total flux measurement.

Before cross-matching the AS2COSMOS and COSMOS2015 catalogues, we estimate the probability of a false match as a function of matching radius. We construct a catalogue of 10^4 random positions across the field and cross-match these with the COSMOS2015 source positions. The probability of a false match is estimated at ∼6.6 per cent at a separation of 0.85 arcsec and we adopt this as our matching radius. Cross-matching the AS2COSMOS and COSMOS2015 catalogues, we identify 179/260 matches within 0.85 arcsec, with a median separation of 0.19 arcsec (false-match probability ∼0.4 per cent). Note that we correct a small astrometric offset between the catalogues of 0.08 ± 0.01 arcsec in R.A., but do not find a significant offset in declination. We comment that the three SMGs that are offset by 0.70–0.85 arcsec to an associated optical counterpart appear morphologically complex and/or faint in the *K*-band imaging, consistent with the expectation that there will be significant systematic offsets ($\sigma \sim 0.3$ arcsec; Chen et al. 2015) between the rest-frame far-infrared and optical emission in these heavily obscured sources (see Fig. 4).

The $YJHK_s$ imaging provided in the COSMOS2015 catalogue is derived from the second data release (DR2) of the Ultravista survey (McCracken et al. 2012). The fourth data release from the Ultravista survey provides imaging (FWHM = 0.8 arcsec) that is up to ∼0.5 mag deeper than the earlier DR2 imaging; the DR4 imaging has a limiting depth of $K_s = 26.4$–25.4 and 25.3–25.1 mag (3σ depth in 2-arcsec diameter aperture) in four ultra-deep and deep stripes, respectively. To improve upon the near-infrared photometry of the AS2COSMOS sources, we replace the $YJHK_s$ COSMOS2015 photometry with 2-arcsec aperture photometry extracted at the position of each SMG on the DR4 imaging. The associated background level and uncertainty on our aperture flux densities are estimated in a 1 arcmin × 1 arcmin region centred on each SMG. To convert our aperture flux densities to a total flux density, we calibrate our results to those in the COSMOS2015 catalogue; for the SMGs with a counterpart in the COSMOS2015, we determine the median ratio between the DR4 aperture flux density and the COSMOS2015 total flux and apply this as an aperture correction to our measurements. Note that we visually inspect the near-infrared imaging and discard photometry for 18 SMGs where the aperture flux is strongly contaminated by a neighbouring, likely to be foreground, source. This leaves us with a sample of 232/260 (88 per cent) SMGs that have detectable emission above 3σ in the K_S band.

In addition, the second data release (Aihara et al. 2019) of Hyper-SuprimeCam (HSC) Subaru Strategic Program (SSP) provides *g*, *r*, *i*, *z*, and *Y* imaging (∼0.6 arcsec seeing) of the COSMOS field at a 3σ equivalent depth of 28.1, 27.9, 27.9, 27.4, and 26.4 mag, respectively. This imaging reaches ∼1 mag deeper than the optical imaging used in the COSMOS2015 catalogue and we include it in our analysis. The HSC-SSP data release provides aperture-corrected flux densities (2-arcsec diameter aperture) for all sources detected at $\geq 5\sigma$ in any of the *g*, *r*, *i*, *z*, or *Y* images. We cross-match the HSC-SSP catalogue to the AS2COSMOS source positions, adopting the same 0.85-arcsec matching radius. This yields 158 optically detected counterparts to the AS2COSMOS SMGs, 20 of which are not present in the COSMOS2015 catalogue. Where a source lacks an entry in the HSC-SSP catalogue, we visually assess the cause using *gri* thumbnail images from the HSC archive and determine if the source is undetected, in which case we adopt the appropriate magnitude limits, or if it is blended with or obscured by a bright nearby source (where we remove the photometry – although this only applies to ∼10 sources and we confirm that it does not influence their best-fitting SEDs derived in Section 2.6).

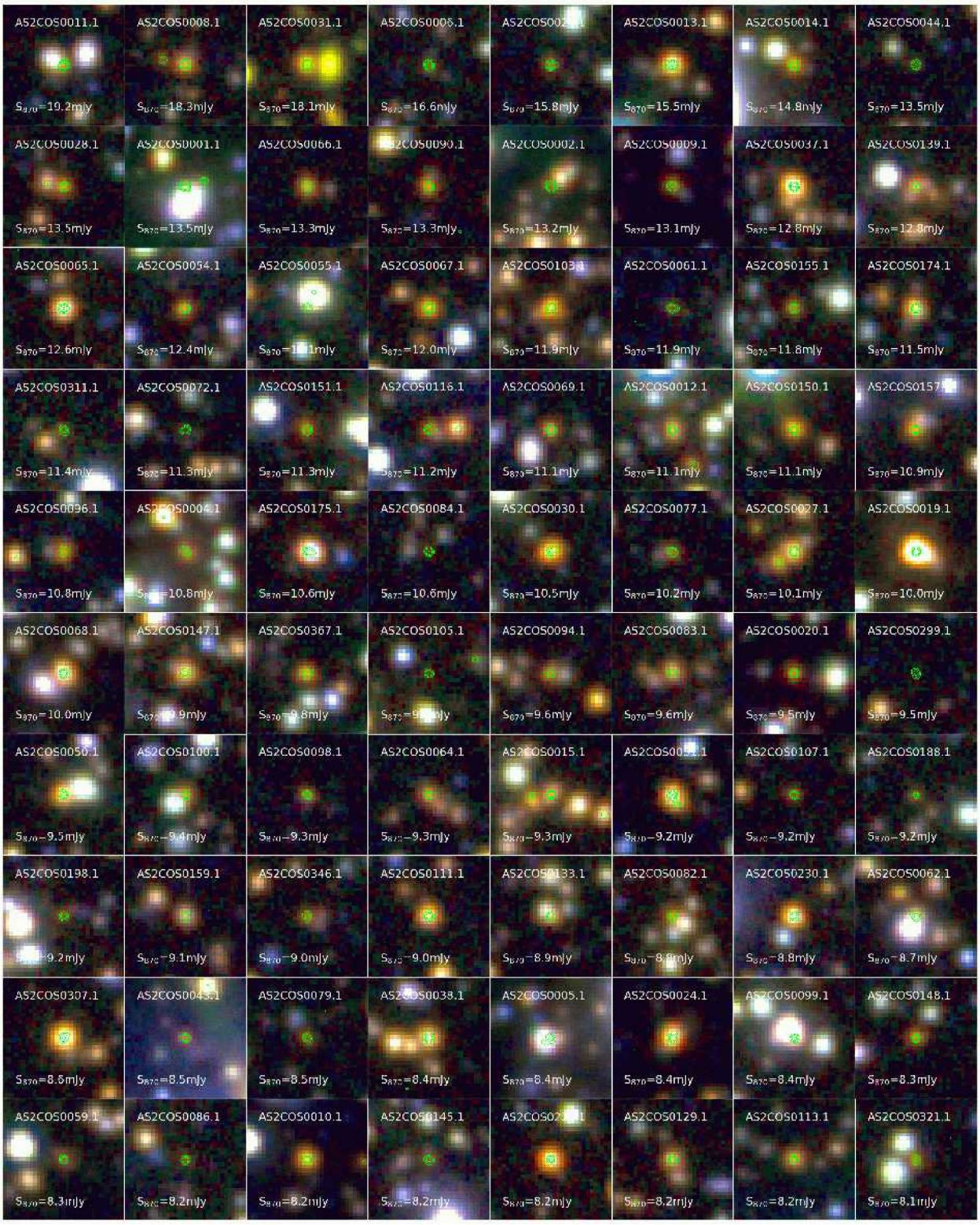

Figure 4. 20 arcsec × 20 arcsec images showing the K_s, 3.6- and 4.5-μm (corresponding to BGR channels) colour images for the 80 brightest 870-μm SMGs ($S_{870\,\mu m} \geq 8.1$ mJy) in the AS2COSMOS sample (the remaining SMGs are shown in Fig. A1). Each of the images is centred on the ALMA source position and are ordered by decreasing ALMA 870-μm flux density. Contours represent that the ALMA 870-μm detections are overlaid at 4σ, 10σ, 20σ, and 50σ. These images demonstrate that the AS2COSMOS SMGs are typically very red and/or faint at near-to-mid-infrared wavelengths, relative to the field population. We find that 9 ± 1 per cent of the AS2COSMOS SMGs are not detected in the Ultravista/K_s imaging, at the $>5\sigma$ significance level, but note that all but one of these sources are detected in the deblended IRAC imaging (median $m_{4.5} = 23.5 \pm 0.2$). Overall, the AS2COSMOS SMGs have red $K_s - 4.5$ μm colours, a median of 1.24 ± 0.04 mag, reflecting the importance of sensitive mid-infrared imaging for conducting an unbiased study of the stellar emission of 870- μm-luminous sources.

2.5.2 *Mid-infrared imaging*

Mid-infrared imaging at 3.6, 4.5, 5.8, and 8.0 μm of the COSMOS field is provided by the *Spitzer* Large Area Survey with Hyper-SuprimeCam (SPLASH; see Steinhardt et al. 2014; Laigle et al. 2016). The SPLASH imaging is comprised of data that were obtained with the Infrared Array Camera (IRAC; Fazio et al. 2004) onboard the *Spitzer Space Telescope* as part of the SPLASH-COSMOS, *Spitzer*-COSMOS (S-COSMOS), *Spitzer* Extended Deep Survey (SEDS), and *Spitzer*-CANDELS data sets, and provides coverage at 3.6–8.0 μm for all AS2COSMOS SMGs. The IRAC data reach an average 3σ limiting magnitude for point sources of 23.9, 23.6, 22.5, and 22.0 mag at 3.6, 4.5, 5.8, and 8.0 μm, respectively.

The resolution of the IRAC imaging (FWHM $\sim$ 2 arcsec) is significantly coarser than the optical-to-near-infrared imaging of the field, and more sophisticated methods than simple aperture photometry are required to derive accurate flux densities for the AS2COSMOS SMGs. For the COSMOS2015 catalogue, deblended IRAC flux densities were determined for all optically selected sources using IRACLEAN (Hsieh et al. 2012). Briefly, IRACLEAN deblends the IRAC imaging using a higher resolution image as a prior, in this case, the stacked $zYJHK_S$ 'detection' image. The IRAC PSF is constructed dynamically across the field and each image is deblended following a process that is functionally identical to CLEAN deconvolution in radio interferometry. To estimate deblended IRAC photometry for the AS2COSMOS SMGs, we again use IRACLEAN but update the prior to include all AS2COSMOS SMGs, including those not formally detected in the $zYJHK_S$ stack. We follow an identical deblending procedure to that described in Laigle et al. (2016), and refer the reader to that work for further details (see also Hsieh et al. 2012). The red colours of the SMG population mean that these bands provide the highest detection rate for our targets, with 238 of the 260 sources detected at 4.5 μm.

2.5.3 *Far-infrared imaging*

Far-infrared imaging of the COSMOS field was obtained at 24 μm with the Multiband Imaging Photometer (MIPS) onboard the *Spitzer Space Telescope*, and at 100 and 160 μm with the Photodetector Array Camera and Spectrometer (PACS; Poglitsch et al. 2010) onboard the *Herschel Space Observatory*. The 24-μm data are taken from the COSMOS-*Spitzer* programme (Sanders et al. 2007) and reach a 1σ depth of $\sim$15 μJy (Le Floc'h et al. 2009). The 100- and 160-μm imaging that was obtained as part of the PACS Evolutionary Probe (PEP) survey has a 1σ sensitivity of $\sim$1.4 and 3.5 mJy, respectively (see Berta et al. 2011, but also Jin et al. 2018).

Source confusion is a concern in the low-resolution MIPS and PACS imaging (FWHM = 6–12 arcsec) and to estimate accurate flux densities for individual sources the emission in the maps must be deblended based on the positions of a prior catalogue. In this work, we primarily utilize the 'superdeblended' catalogue presented by Jin et al. (2018), which contains deblended 24–160-μm photometry for K_s- and 3-GHz-selected sources in the COSMOS field. Briefly, Jin et al. (2018) deblend the MIPS and PACS imaging of the field by PSF fitting at the position of 194 428 sources in their prior catalogue following the methodology presented by Liu et al. (2018). Cross-matching the optical and radio counterparts to the AS2COSMOS SMGs with the Jin et al. (2018) catalogue yields 24–160-μm photometry for 228/260 AS2COSMOS SMGs.

The source catalogue presented by Jin et al. (2018) is incomplete to far-infrared-luminous, but radio- and/or K_s-faint, sources. To increase the completeness level of our 24–100-μm photometry, we also match to the source catalogue from the PACS/PEP survey (Lutz et al. 2011; see also Magnelli et al. 2013) that was constructed using a 24-μm-only prior list. We find an additional seven counterparts to the AS2COSMOS SMGs, within a matching radius of 2 arcsec (see Chen et al. 2016), increasing the overall completeness level for the AS2COSMOS SMGs to 235/260.

Imaging at 250, 350, and 500 μm of COSMOS was taken with the Spectral and Photometric Imaging Receiver (SPIRE; Griffin et al. 2010) onboard the *Herschel Space Observatory* as part of the *Herschel* Multitiered Extragalactic Survey (Oliver et al. 2012). These data are particularly important for our analysis as they are expected to sample the peak of the rest-frame dust emission from the AS2COSMOS SMGs ($\lambda_{\rm obs} \sim 300$ μm for a source with a characteristic dust temperature of 30 K at $z \sim 2.5$) and, as such, constrain the total infrared luminosities of our sample. Due to the coarse resolution of the *Herschel* SPIRE imaging (FWHM = 18–35 arcsec), source deblending is again crucial for determining accurate flux densities for each of the AS2COSMOS SMGs.

We deblend the 250-, 350-, and 500-μm imaging following the method described in Swinbank et al. (2014). Briefly, we construct a prior list of MIPS/24 μm, VLA/3 GHz (see Section 2.6), and ALMA/870 μm sources that are used to deblend the low-resolution maps. The typical K_s-selected sources included by Jin et al. (2018) in the deblending of the 24–160-μm imaging are not expected to be luminous in the SPIRE imaging and, as such, we omit these from our prior list. Deblending of the SPIRE maps is achieved by PSF fitting to the observed flux densities at the position of all sources in the prior catalogue. To avoid 'overdeblending', the maps were deblended in order of increasing wavelength with only ALMA SMGs and/or sources detected at $>2\sigma$ in the proceeding map retained in the prior list for deblending the next longer wavelength map. The associated uncertainties on the deblended flux densities, and detection limits of the SPIRE maps, were determined through extensive Monte Carlo simulations to inject and recover simulated sources in each map. We find that the deblended 250-, 350-, and 500-μm maps reach a typical 3σ limit for detection of 7.4, 8.1, and 10.6 mJy, respectively.

Overall, we find that 235/260 of the AS2COSMOS SMGs are detected in at least one waveband between 24 and 500 μm, with 222/260 (85 per cent) in at least one band between 100 and 500 μm. To first order, the high detection fraction for the AS2COSMOS SMGs at 100–500 μm reflects our selection of bright single-dish sources for ALMA follow-up observations. Indeed, the 38 SMGs without a detection in either the PACS or SPIRE imaging have a median 870-μm flux density of $S_{870\,\mu{\rm m}} = 4.1 \pm 0.5$ mJy, significantly fainter than the median flux density of $S_{870\,\mu{\rm m}} = 7.1 \pm 0.2$ mJy for the 'detected' subset.

2.5.4 *Radio*

To analyse the radio properties of the AS2COSMOS SMGs, we utilize deep 3-GHz imaging of COSMOS undertaken in a Large Project with the Karl. G. Jansky Very Large Array (Smolčić et al. 2017). Briefly, the 3-GHz map of the COSMOS field reaches a median sensitivity of 2.3 μJy, at a resolution of 0.75 arcsec, over 2 deg^2. In the following, we use the source catalogue presented by Smolčić et al. (2017), which contains total flux densities for 10 830 sources that were identified at the $>5\sigma$ significance level.

We cross-correlate the AS2COSMOS and VLA/3-GHz catalogues and identify 191 counterparts to the AS2COSMOS SMGs within a matching radius of 1 arcsec. The adopted matching radius is comparable to that used to identify optical counterparts to each of the SMGs and, considering random positions in the field, we estimate a false-match probability of ∼0.1 per cent. Note that extending the matching radius to 2 arcsec does not yield any further unique 3-GHz counterparts. A visual inspection the VLA imaging shows that two pairs of SMGs with a small on-sky separation (∼1–2 arcsec) have distinct, well-separated, peaks (SNR = 18–33) in the 3-GHz map, but they are grouped into a single source in the VLA/3-GHz catalogue. To obtain deblended 3-GHz flux densities for these SMGs (AS2COS 0051.1/.2 and 0228.1/.2), we use the CASA/IMFIT routine to simultaneously model the emission from each pair of components. Overall, we identify 3-GHz counterparts to 193/260 AS2COSMOS SMGs with flux densities of 12–650 μJy.

To investigate the radio properties of the 3-GHz-faint SMGs, we stack thumbnails extracted from the VLA map at their positions. These 67 SMGs are detected at the 27σ level in the stacked image with an average peak flux density of 8.1 ± 0.3 μJy, placing the average source marginally below the formal limit for detection in the VLA map (∼11.5 μJy). Motivated by the strength of the stacked emission, we estimate the 3-GHz flux density of each of the radio-faint SMGs by extracting the pixel flux density at the position of each source in the VLA map: The 3-GHz maps are calibrated in units of μJy per beam and the pixel value represents the total flux density for an unresolved source at a given position. At the resolution of the VLA imaging, we expect that the radio emission from the AS2COSMOS SMGs will be marginally resolved (intrinsic FWHM ∼ 0.6 arcsec; e.g. Biggs & Ivison 2008; Miettinen et al. 2015; Thomson et al. 2019) and, as such, our simple flux estimates will systematically underestimate the total flux of each source. To correct for this effect, we compare the pixel and total flux densities for the 193 AS2COSMOS SMGs with counterparts in the VLA/3-GHz catalogue. We determine a median total-to-peak flux density ratio of 1.21 ± 0.03 for the average SMG, which we use to correct our flux estimates for the 67 3-GHz-faint SMGs to a total flux density.

2.5.5 *X-ray*

The *Chandra* COSMOS Legacy Survey (Civano et al. 2016) provides coverage of the AS2COSMOS SMGs in the 0.5–2-keV (soft) and 2–10-keV (hard) bands at an effective exposure of 160 ksec across our full survey area. The source catalogue for the survey contains 4016 point sources that are detected in any combination of the soft, hard, and full (0.5–10 keV) bands (flux limit of 8.9×10^{-16} erg s^{-1} cm^{-2} in the full band).

Matching the *Chandra* and ALMA source catalogues within the 3σ positional uncertainties on the X-ray positions, we identify 24 counterparts to the AS2COSMOS SMGs, at a median positional offset of 0.56 ± 0.08 arcsec. Note that we choose to include a 'match' to AS2COSMOS308.1 despite the X-ray source lying offset to the ALMA position at a 4.8σ significance level. The offset between the X-ray and ALMA positions is 0.84 arcsec (i.e. 1/3 of the on-axis *Chandra* beam) and a visual inspection of the optical-to-near-infrared imaging indicates that there is no clear alternative counterpart to the source at optical-to-radio wavelengths.

We also cross-correlated the AS2COSMOS sources with the *XMM–Newton* X-ray survey of COSMOS by Brusa et al. (2010), but find no additional reliable identifications.

2.6 Panchromatic SED fitting

We first summarize the detection rates for the AS2COSMOS SMGs in the various wavebands discussed above. Other than at 870 μm, the highest detection rate is found in the *Spitzer* IRAC bands with 238 of the 260 SMGs with $\geq 3\sigma$ detections in the 4.5-μm band. The detection rate drops markedly in bluer wavebands, as has been seen for previous studies of this dusty and typical high-redshift population, with 196 sources and 103 being detected above 3σ in the *Y* and *B* bands, respectively. However, at longer wavelengths, 174 of the 260 SMGs have $\geq 3\sigma$ detections at 350 μm from the deblended photometry. Overall, the median number of photometric detections for the SMG's SEDs come from 18 bands, with the maximum being 24 and just 5 SMGs have detections in five or fewer bands to use (along with limits) to constrain their SEDs. The detection rates in K_S 3.6 and 350 μm of 89, 92, and 67 per cent are slightly higher than the corresponding values of 83, 90, and 59 per cent for the AS2UDS study of Dudzevičiūtė et al. (2020) to which we compare our results.

Having collated the multiwavelength observations of our ALMA-identified SMG sample, we now use the MAGPHYS SED modelling programme (da Cunha et al. 2008, 2015; Battisti et al. 2019) to fit the multiwavelength SEDs of these sources. Our approach here is to match the method used in the analysis of ∼700 ALMA-identified SMGs from the AS2UDS survey by Dudzevičiūtė et al. (2020), to allow us to easily compare the physical properties estimated by MAGPHYS for that sample to the typically more luminous sources studied here.

We refer the reader to Dudzevičiūtė et al. (2020) for a detailed description of the application and testing of the MAGPHYS software on large samples of observed and theoretical galaxy SEDs, with a particular focus on dust-obscured star-forming galaxies. These include testing of the precision of the derived photometric redshifts using a sample of ∼7000 spectroscopically identified galaxies at $z \sim 0$–5 in the UKIDSS UDS field, including 44 SMGs. From the spectroscopic comparison, they determine $\Delta z/(1 + z_{\rm spec}) = -0.02 \pm 0.03$, with a 16–86th percentile range in $\Delta\ z/(1 + z_{\rm spec})$ of −0.16 to 0.10. This photometric redshift accuracy is comparable to that found for SMGs in the COSMOS field by Battisti et al. (2019). Dudzevičiūtė et al. (2020) also provide an assessment of the systematic uncertainties in other physical parameters from MAGPHYS through its application to model galaxy SEDs for strongly star-forming galaxies selected from the EAGLE simulation (McAlpine et al. 2019). Here we provide a brief description of this analysis; full details are given in Ikarashi et al. (in preparation).

We used the latest version of MAGPHYS (Battisti et al. 2019), which is optimized to fit SEDs of high-redshift, star-forming galaxies and can provide estimates of the redshifts of the sources based on the SED fitting. MAGPHYS employs an energy balance technique to combine information from the attenuation of the stellar emission in the UV/optical and near-infrared by dust, and the reradiation of this energy in the far-infrared. This is a particular advantage for modelling the photometric redshifts of very obscured galaxies such as SMGs, where there may be relatively few constraints available from the optical and near-infrared SED shape due to the dust obscuration.

To fit to the observed SED galaxy, MAGPHYS generates a library of model SEDs for a grid of redshifts for each star formation history considered. The code selects models that best fit the multiwavelength photometry by matching the model SEDs to the data using a χ^2 test and returns the respective best-fitting parameters; most importantly, it provides a median redshift from the probability

distribution function (PDF) from the best-fitting models as well as the full PDF of the redshifts. We discuss the photometric redshifts derived from our MAGPHYS analysis in Section 3.5 and the other physical properties of the luminous SMGs from AS2COSMOS in Ikarashi et al. (in preparation).

3 RESULTS AND DISCUSSION

We start by discussing the basic properties of the sample as illustrated in Fig. 4. Most noticeable in these K_S 3.6- and 4.5-μm colour images is the typical faintness and the red colours of the majority of the SMGs (even in this combination of near- and mid-infrared filters) compared to the general field population in these fields. Next, we note several examples where the SMG lies very close to bright and blue galaxies, which are likely foreground (e.g. AS2COS 0011.1, AS2COS 0001.1, and AS2COS 0062.1). These may include examples of gravitationally lensed systems, although the typical separation of the SMG from the putative lens suggests that few of them are examples of strongly lensed (multiply imaged) systems with the highest amplifications. Instead, the expected lens boosts are likely to be modest: ∼1.2–3 × (see Section 3.4 for an example). Finally, in the fields that show two or more SMGs, there is a visual impression that these preferentially display separations of ∼2–5 arcsec, and a more quantitative analysis suggests a strong excess of pairs of sources on scales of $\lesssim$3 arcsec (corresponding to ∼20–30 kpc at typical redshifts for SMGs). This characteristic scale is smaller than the ALMA primary beam and if real could either be a signature of lensing, or it could be indicating a natural scale for peak activity of interacting galaxies. We will discuss this issue further in Ikarashi et al. (in preparation). We note that there is a rapid increase in the apparent presence of companion SMGs in the thumbnails showing the fainter sources, but this is simply a result of the fact that these SMGs only come to be in our bright single-dish-selected sample through their presence in the field of a second, brighter SMG.

3.1 Number counts

The number of sub-millimetre emitters as a function of flux density, i.e. the number counts, is a basic observable property that can provide constraints on models of galaxy formation (e.g. Baugh et al. 2005). The brighter sources in the AS2COSMOS sample have a relatively simple selection function (see Fig. 2) and, as such, the sample is well suited to constrain the bright end of the 870-μm number counts. We determine these AS2COSMOS number counts here and compare our results to previous surveys of luminous SMGs.

In Fig. 5 and Table 2, we present the cumulative and differential number counts derived from the AS2COSMOS source catalogue. The counts are constructed to a lower flux limit of 6.2 mJy, corrected for sample incompleteness using the completeness curve determined for the sample in Section 2.4 (see Fig. 2), and normalized to the 1.6-deg^2 area of the S2COSMOS MAIN survey. The associated uncertainties on the AS2COSMOS counts were estimated by constructing 10^4 realizations of the AS2COSMOS source catalogue. In each realization, we randomly assigned a flux density to each AS2COSMOS SMG based on its measured value and associated uncertainty and reconstructed the counts. The 16–84th percentile of the resulting distribution was combined with the expected Poisson uncertainty (Gehrels 1986) to provide an estimate of the total uncertainty on each bin in the counts.

We find that both the AS2COSMOS cumulative and differential counts follow a smooth, near-exponential decline between $S_{870\,\mu m}$ = 6.2 and 20 mJy. As shown in Fig. 5, the AS2COSMOS cumulative counts are in good agreement with those derived for the S2COSMOS survey – once allowance has been made in the latter for the effects of boosting and blending based on a model with a representative functional form for the intrinsic counts. While a comparison to the *raw* uncorrected S2COSMOS counts shows that they are ∼31 ± 8 per cent higher at the survey limit. We note that the ALMA cumulative counts are marginally *higher* than those estimated from the corrected single-dish survey at ∼10 mJy, indicating the limitations of the end-to-end modelling technique (which disregards clustering) to account for blending, although any differences seen are at the <3σ significance level (after accounting for the contribution from Poisson noise to the associated uncertainties). The agreement between the ALMA and the SCUBA-2 counts is consistent with our earlier result that the brightest SMG in each AS2COSMOS map accounts for, on average, all of the deboosted and deblended flux density of the targeted SCUBA-2 source (see Fig. 3) – showing that those statistical corrections are reliable on average, if the approximate form of the counts is already known.

Previous interferometric follow-up observations of single-dish-identified sub-millimetre sources have also reported reductions in the normalization of the interferometric counts, relative to the parent single-dish sample (e.g. Karim et al. 2013; Simpson et al. 2015b; Hill et al. 2018; Stach et al. 2018). For example, Stach et al. (2018) present the number counts derived from the AS2UDS survey of 714 SCUBA-2 sources in the UDS field, and report a 28 ± 2 per cent (41 ± 8 per cent) reduction in the counts at >4 mJy (>7 mJy), relative to the parent single-dish sample. This is broadly consistent with the reduction we find when comparing the uncorrected S2COSMOS counts to those derived here, as expected given our result below that the parent samples for both surveys suffer a comparable level of source blending (see Section 3.3).

Fig. 5 also shows that our ALMA-derived counts in the COSMOS field lie a factor of 1.4–2.0× higher than those from AS2UDS or the SMA study of bright S2CLS sources by Hill et al. (2018). This difference corresponds to a formal significance of ∼2.3σ at the limit of AS2COSMOS. However, as we show in Section 3.2, these studies are broadly consistent when allowance is made for the cosmic variance in the counts derived from similar sized areas drawn from simulations created using the GALFORM semi-analytic galaxy formation model.

To provide a simple parametrization of the sub-millimetre number counts, we now determine the best-fitting model to both the AS2COSMOS counts and prior estimates of the sub-millimetre counts based on sensitive ALMA observations in the literature. At the bright end of the counts ($\gtrsim$4 mJy), we include in our analysis the estimates of 870-μm counts from the ALESS and AS2UDS surveys (Karim et al. 2013; Stach et al. 2018), and extend our analysis to fainter fluxes by including the estimate of the 870-μm counts from the ALMACAL survey (Oteo et al. 2016) and the 1.2-mm counts from the ASAGAO survey (Hatsukade et al. 2018; see also Dunlop et al. 2017; Franco et al. 2018). The 1.2-mm counts are converted to 870 μm assuming a modified blackbody with $\beta = 1.8$ and a dust temperature of 32 K, at a redshift of $z = 2.6$ (e.g. Dudzevičiūtė et al. 2020; $S_{870\,\mu m}/S_{1200\,\mu m} = 2.7$). We assume that the sub-millimetre counts follow a simple Schechter function of the form

$$\frac{dN}{dS} = \frac{N_0}{S_0}\left(\frac{S}{S_0}\right)^{-\gamma} \exp\left(\frac{-S}{S_0}\right), \quad (1)$$

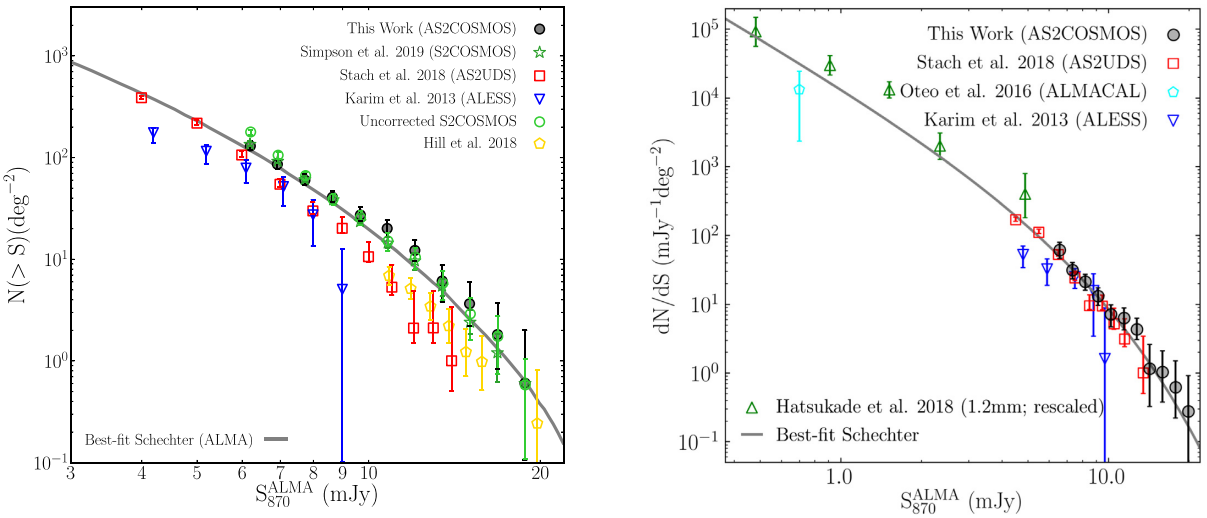

Figure 5. *Left:* The cumulative 870-μm number counts constructed from the AS2COSMOS pilot survey, compared to those constructed from the parent single-dish SCUBA-2 sample and other interferometric surveys. We find that both the shape and normalization of the AS2COSMOS counts are in good agreement with those from the S2COSMOS survey after corrections are applied to the latter to account for boosting and blending (Simpson et al. 2019); for illustration, we are also showing the number counts of sources from S2COSMOS without these corrections. The AS2COSMOS counts are marginally higher than the boosting/blending-corrected single-dish counts at ∼10 mJy, but we stress that any difference is at the $<3\sigma$ significance level. For a comparison, we also show the counts constructed from prior ALMA studies of LABOCA-selected sources in the ECDFS (ALESS; Karim et al. 2013), SCUBA-2-selected sources in the UDS (AS2UDS; Stach et al. 2018), and the SMA-follow-up of bright SCUBA-2 sources from S2CLS (Hill et al. 2018). The AS2COSMOS counts are a factor of ∼1.4–2.0× higher than those constructed from AS2UDS or the study of Hill et al. (2018) (which includes the sources in the AS2UDS pilot published by Simpson et al. 2015a), but they are consistent within the associated uncertainties at the $<2.3\sigma$ significance level, before considering the effects of cosmic variance (see Section 3.2). *Right:* Similar to the left-hand panel but showing the differential 870-μm number counts constructed from AS2COSMOS pilot and published ALMA surveys. We also show the counts constructed from deeper, small-area surveys with ALMA that were conducted around either calibrator fields (ALMACAL; Oteo et al. 2016) or as a blank-field mosaic (ASAGAO; Hatsukade et al. 2018). The differential counts from the various ALMA surveys decline smoothly from $S_{870\,\mu m} = 0.4$ to 20 mJy and are well described by a single Schechter function. Overall, we highlight that the AS2COSMOS pilot survey detects 108 (39) SMGs at $S_{870\,\mu m} > 7\,(10)$ mJy, and represents a factor of ∼2× increase in sample size relative to the largest previous studies.

Table 2. AS2COSMOS number counts.

S_{870} (mJy)	$N\,(>S_{870})$ (deg^{-2})	S_{870} (mJy)	dN/dS_{870} (deg^{-2} mJy^{-1})
6.2	130^{+13}_{-12}	6.6	$61.4^{+20.0}_{-16.0}$
6.9	$85.9^{+9.5}_{-8.7}$	7.3	$31.2^{+10.0}_{-8.0}$
7.7	$60.4^{+7.4}_{-6.7}$	8.2	$21.2^{+6.0}_{-5.2}$
8.6	$40.9^{+5.8}_{-5.2}$	9.2	$13.1^{+4.2}_{-3.6}$
9.7	$27.6^{+4.8}_{-4.2}$	10.2	$7.1^{+2.7}_{-2.4}$
10.8	$20.1^{+4.1}_{-3.6}$	11.4	$6.3^{+2.5}_{-2.0}$
12.1	$12.2^{+3.3}_{-2.6}$	12.8	$4.3^{+1.9}_{-1.3}$
13.5	$6.1^{+2.7}_{-2.3}$	14.3	$1.2^{+1.4}_{-0.8}$
15.1	$3.7^{+2.3}_{-1.5}$	15.9	$1.0^{+1.1}_{-0.7}$
16.8	$1.8^{+1.9}_{-1.0}$	17.8	$0.6^{+0.9}_{-0.4}$
18.8	$0.6^{+1.4}_{-0.5}$	19.9	$0.3^{+0.6}_{-0.2}$

Note. The cumulative and differential number counts at 870 μm constructed from the AS2COSMOS survey of the central 1.6 deg^2 of the COSMOS field. The cumulative count bin fluxes are at the lower limit of the bin and the differential count fluxes refer to the bin centres.

and determine best-fitting parameters of $N_0 = 2770^{+1560}_{-650}$ deg^{-2}, $S_0 = 4.2^{+0.5}_{-0.8}$ mJy, and $\gamma = 2.3^{+0.1}_{-0.3}$. As can be seen in Fig. 5 the best-fitting parametrization provides a reasonable description of the observed counts (reduced $\chi^2 = 1.5$) at $S_{870\,\mu m} = 0.4$–20 mJy, although we note that the faint end of the counts ($\lesssim$4 mJy) is constrained by a modest number of source (∼40–50) and that this is reflected in the significant associated uncertainties on our best-fitting model parameters.

3.2 Cosmic variance

Since the discovery of the SMG population, it has been speculated that these intensely star-forming systems may be the progenitors of local spheroidal galaxies (e.g. Lilly et al. 1999; Blain et al. 2004; Swinbank et al. 2006, 2010a; Tacconi et al. 2008; Simpson et al. 2014; Dudzevičiūtė et al. 2020). Under the ΛCDM paradigm, SMGs would thus represent a biased tracer of the underlying mass distribution of the Universe (e.g. Hickox et al. 2009), which we would expect to manifest as excess field-to-field variance in the integrated 870-μm number counts (Scott et al. 2012).

Exploiting the AS2COSMOS and AS2UDS surveys, we can investigate whether the interferometrically identified SMG population (so unaffected by blending) shows evidence for cosmic variance as a function of both 870-μm flux density and survey area. The AS2COSMOS and AS2UDS surveys are homogenous and, taken together, provide a catalogue of 223 bright SMGs ($S_{870\,\mu m} > 6.2$ mJy) selected over a survey area of 2.6 deg^2, corresponding to a survey volume of 0.12 Gpc^3 if we assume a maximal redshift range for the SMG population of $z \sim 1$–5 (see Section 3.5, but also Simpson et al. 2014; Strandet et al. 2016; Dudzevičiūtė et al. 2020).

To investigate the effect of cosmic variance on the bright 870-μm ALMA number counts, we first sub-divide the AS2COSMOS and

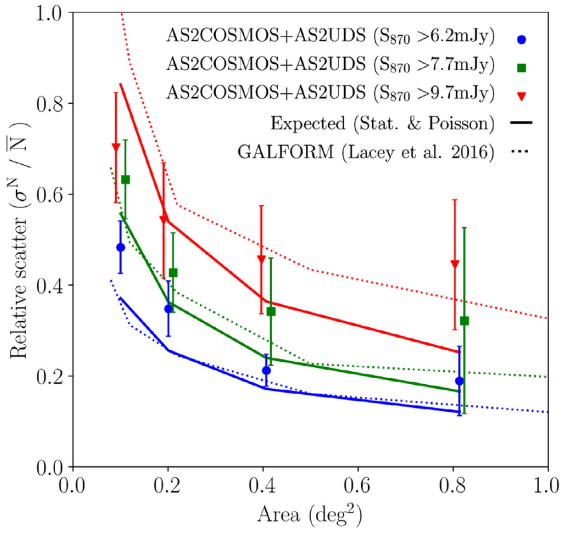

Figure 6. The fractional scatter in the cumulative 870-μm number counts as a function of survey area and flux limit: $\sigma^N/\bar{N}$. Number counts were constructed from sub-areas of the AS2COSMOS and AS2UDS surveys and the scatter in the results, σ^N, is normalized to the sample mean, $\bar{N}$. The expected scatter in the observed counts is represented by a solid line and reflects the contribution from both statistical (e.g. flux uncertainties) and Poissonian uncertainties. We find an enhancement in the relative scatter of the cumulative counts that can be attributed to cosmic variance of ∼30 per cent in the $S_{870\,\mu m} > 6.2$ mJy population in survey areas of $\lesssim$0.2 deg^2, although we caution that the significance of the result is modest. For a comparison, we show the total scatter estimated from the GALFORM semi-analytic model of galaxy formation (dotted line). The predictions of the GALFORM model are broadly consistent with the results presented here, and suggest that the observed $\gtrsim$1.4× difference between the cumulative source counts in the AS2COSMOS and AS2UDS surveys could be simply due to cosmic variance.

AS2UDS surveys into 26 independent regions each with an area of ∼0.1 deg^2. These sub-regions were then combined to provide a sample of representative surveys over 0.1–0.8 deg^2. For each sub-field, we derived the completeness-corrected, integrated counts and estimated the total variance in the resulting distribution, normalized to the sample mean: $\sigma^N/\bar{N}$. The total variance in the counts is comprised of contributions from cosmic variance, Poisson errors, and statistical uncertainties (e.g. flux density estimates). To estimate the statistical uncertainty on the distribution of counts, we use a set of Monte Carlo simulations, comprising 10^3 realizations of the integrated counts for each sub-field. The expected Poisson uncertainty is estimated following Gehrels (1986).

In Fig. 6, we show the total variance in the cumulative number counts as a function of survey area, as well as in three bins of the AS2COSMOS 870-μm counts ($S_{870\,\mu m} > 6.2$, 7.7, and 9.7 mJy). As expected, the total field-to-field variance in the 870-μm counts increases in smaller areas and at higher flux densities. At $S_{870\,\mu m} > 6.2$ mJy, we estimate that the total normalized variance in the counts decreases from 48 ± 6 per cent over survey regions of 0.1 deg^2 to ∼20 per cent at 0.4–0.8 deg^2 (21 ± 4 per cent at 0.4 deg^2). To isolate any potential contribution from cosmic variance, we subtract the estimated statistical and Poissonian uncertainties from the total variance, as a function of survey area and flux density (see Fig. 6). We estimate cosmic variance of ∼30 and ∼20 per cent in the >6.2 mJy population for survey areas of 0.1 and 0.2 deg^2, respectively, but caution that the excess variance is only significant at the $\lesssim 2\sigma$ level (1.9σ and 1.6σ, respectively). If we consider larger survey areas, or brighter flux limits, then we determine that the total variance is systematically elevated, relative to that expected from Poisson uncertainties and other errors, but again this is at the $\ll 1\sigma$ significance level.

To assess how the variance we measure compares to that expected from theoretical models, we use results from the GALFORM semi-analytic model of galaxy formation (Lacey et al. 2016). We construct a 20 deg^2 of model sub-millimetre sky using GALFORM, in five distinct light-cones, and estimate the normalized variance in the integrated number of simulated SMGs in sub-regions spanning 0.1–1.0 deg^2. The GALFORM simulations do not include any statistical uncertainties and as such, to ensure consistency with the observational results, we add our estimate for the statistical variance on the AS2COSMOS + AS2UDS sample to the measured variance in the simulation. As shown in Fig. 6, the predictions from GALFORM are broadly in line with our observational results, although we note that the variance in the simulation lies systematically below our observational result for the $S_{870\,\mu m} > 6.2$ mJy population on 0.1–0.2-deg^2 scales (this may be explained by the number of simulated sources being higher than observed, so the relative Poisson contribution is lower). We also note that the observed AS2UDS counts are a factor of ∼1.4–2.0× lower than those from AS2COSMOS (Fig. 5), which corresponds to a formal significance of ∼2.3σ. However, the ALMA counts in the two fields are broadly consistent with the scatter between degree-sized fields predicted by GALFORM.

We highlight that these empirical limits on the cosmic variance in the counts of SMGs in ∼0.1-deg^2 areas have implications for the searches for overdensities of such sources that rely on identifying the excess in the projected surface density of sources, unless care is taken to assess the significance of above-Poisson variance in the number counts (e.g. Dannerbauer et al. 2014; Casey 2016; Harikane et al. 2019).

3.3 Multiplicity

Using our catalogue of AS2COSMOS sources, we now assess the level of multiplicity in the parent S2COSMOS sample. We follow the convention adopted in prior studies (e.g. Simpson et al. 2015b; Cowie et al. 2018; Stach et al. 2018) and define a single-dish S2COSMOS source as a 'multiple' if two or more SMGs with flux densities of $S_{870\,\mu m} \geq 1$ mJy are identified within the primary beam of the corresponding ALMA map (i.e. within 8.7 arcsec of the SCUBA-2 position). We find one single-dish source that breaks up into four SMG counterparts, 11 that are blends of three SMGs, and a further 51 with two SMG counterparts (e.g. Fig. 1). The highest multiplicity source, S2COSMOS 0003 (Fig. 1), has been previously discussed by Wang et al. (2016), who have shown that the four components all lie in a single structure at $z = 2.50$. We discuss a similar association of dusty star-forming galaxies associated with the highest significance S2COSMOS source, S2COSMOS 0001, at $z = 4.63$ in Section 3.4.

In total, we find that 63 of the 182 AS2COSMOS maps contain two or more SMGs with $S_{870\,\mu m} > 1$ mJy, corresponding to a multiplicity fraction for the sample of 34 ± 2 per cent. These secondary SMGs contribute a median of 30^{+4}_{-2} per cent of the integrated ALMA flux density of all sources in each ALMA map, and we find no evidence that this fraction depends on single-dish flux density in the flux range we probe (Fig. 7). The level of multiplicity in the AS2COSMOS sample is significantly higher than the 11 ± 1 per cent determined by Stach et al. (2018) for the typically fainter AS2UDS sample, or the 13 ± 6 per cent found by Cowie et al.

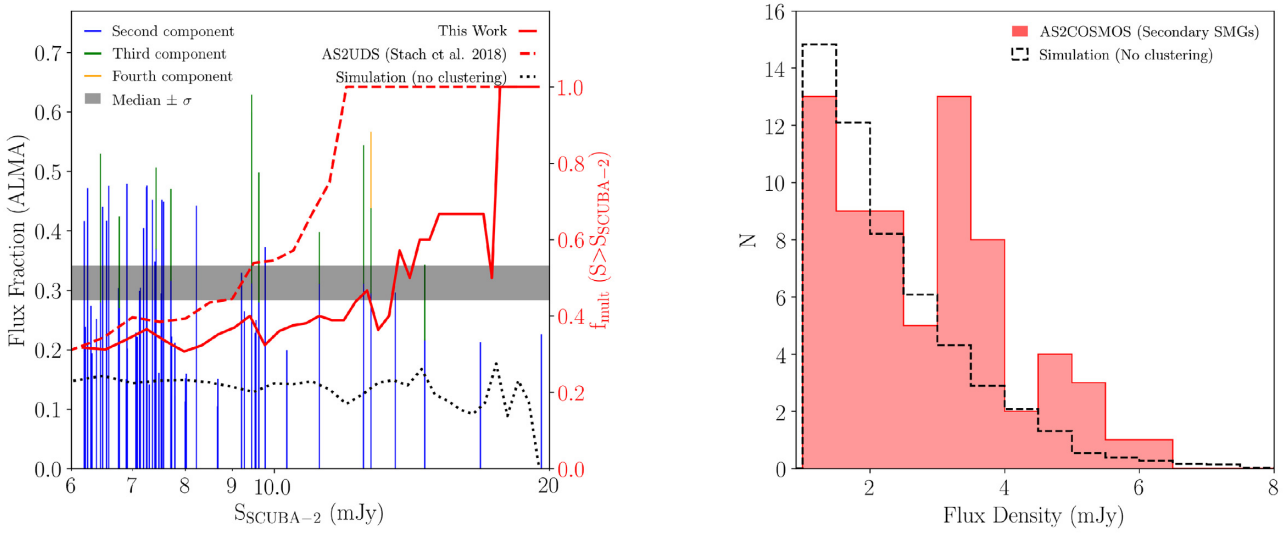

Figure 7. *Left:* The fraction of the integrated ALMA flux density that is contained in secondary components ($S_{870\,\mu m} > 1$ mJy) in each AS2COSMOS map, as a function of the single-dish flux density of the targeted S2COSMOS source. Secondary AS2COSMOS SMGs contribute, on average, 30^{+3}_{-2} per cent (shaded region) of the integrated ALMA flux density with no significant dependence on SCUBA-2 flux density, in good agreement with results from AS2UDS for the same range in flux density (30 ± 1 per cent; Stach et al. 2018). The fraction of AS2COSMOS maps that contain more than one SMG (solid line) shows a weak dependence on single-dish flux density, in broad agreement with the AS2UDS survey (dashed line; Stach et al. 2018). The level of multiplicity in the AS2COSMOS and AS2UDS samples is elevated relative to the expectations of an unclustered population (dotted line), which suggests that ∼30 per cent of the AS2COSMOS 'multiple' maps contain physically associated SMGs. *Right:* The flux density distribution of the 76 secondary SMGs ($S_{870\,\mu m} > 1$ mJy) that are detected within the primary beam of each AS2COSMOS map. For a comparison, we show the expected flux distribution of secondary components from our simulation of the A/S2COSMOS surveys, which assume an unclustered population of sub-millimetre sources. We find that the number density of secondary AS2COSMOS SMGs with flux densities of $S_{870\,\mu m} < 3$ mJy is broadly consistent with the results of our simulation, indicating that these faint SMGs are typically line-of-sight associations to the primary SMG in each ALMA map. However, we find a clear excess in the number density of AS2COSMOS secondaries brighter than $S_{870\,\mu m} \gtrsim 3$ mJy, relative to the simulation, and estimate that 62 ± 7 per cent of these brighter components are physically associated with the primary SMG in their respective maps.

(2018) in their Super-GOODS survey.[3] However, the multiplicity of SCUBA-2 sources has been shown to correlate with their single-dish flux density (Stach et al. 2018), and both the AS2UDS and Super-GOODS samples probe to fainter fluxes that the sources considered here ($S_{870\,\mu m} > 4$ mJy and $S_{870\,\mu m} > 2.2$ mJy, respectively). To provide a fair comparison between the AS2COSMOS and AS2UDS surveys, we estimate the multiplicity of the 88 AS2UDS sources with single-dish flux densities brighter than the selection limit for our pilot AS2COSMOS sample (i.e. $S_{870\,\mu m} > 6.2$ mJy). We do not consider the Super-GOODS sample presented by Cowie et al. (2018) as it contains just four SCUBA-2 sources with flux densities above the S2COSMOS selection limit. For the subset of 88 AS2UDS sources brighter than $S_{870\,\mu m} = 6.2$ mJy, we determine a multiplicity rate of 33 ± 5 per cent (and a median fractional flux in secondaries of 30 ± 1 per cent). This is in very good agreement with our results for AS2COSMOS and confirms the overall agreement between the two surveys.

Our analysis highlights an apparent increase in the multiplicity rate of SCUBA-2 sources between $S_{850\,\mu m} \sim 4$ and 6 mJy (Stach et al. 2018). Interestingly, there is no evidence in the AS2COSMOS sample for a change in the multiplicity of SCUBA-2 sources at >6 mJy (see Fig. 7). To investigate this further, we combine the AS2COSMOS and AS2UDS samples and repeat our analysis on this 50 per cent larger sample. For the combined sample, we again find no trend in the rate of multiplicity with single-dish flux density between $S_{850\,\mu m} = 6$ and 12 mJy (30 ± 2 per cent). However, there is a statistically significant increase in the multiplicity rate to 53 ± 8 per cent for sources at > 12 mJy. Thus, while the frequency of source blending is broadly uniform across the AS2COSMOS sample, we note that it does tend to increase for the most luminous of 850-μm sources.

It is important to note that the AS2COSMOS sample is very incomplete for sources with flux densities as faint as 1 mJy. Hence, our estimate of the multiplicity of SCUBA-2 sources is undoubtedly a lower limit. However, we also stress that assuming the best-fitting parametrization of the sub-millimetre number counts (see Section 3.1) we expected a surface density approximately one SMG brighter than >1 mJy per 4–5 ALMA primary beams (but this rapidly drops to only one per ∼60 ALMA maps at $S_{870\,\mu m} \sim 3$ mJy, the median flux of our sample of secondary SMGs). This indicates that our adopted definition for a 'multiple' is beginning to approach the background population. Accounting for this 'background' contribution would likely steepen the trend of multiplicity with single-dish flux seen in Fig. 7.

To quantify the fraction of AS2COSMOS multiples that likely arise from line-of-sight associations, we use the suite of A/S2COSMOS simulations that were presented in the previous sections. From this ALMA-SCUBA-2 simulation, we estimate that 23 per cent of simulated SCUBA-2 sources with flux densities of >6.2 mJy would be classed as multiples in a follow-up survey equivalent to AS2COSMOS. The input model for the simulation

[3]Source multiplicity is sensitive to the beam size of the parent single-dish observations and the depth and resolution of the follow-up interferometric imaging. As such, we choose to focus our comparison on prior studies that obtained ALMA follow-up observations of SCUBA-2-identified sources but note that comparable results have been obtained in studies of SMGs with other facilities (e.g. Karim et al. 2013; Brisbin et al. 2017; Hill et al. 2018).

does not include clustering and, as such, all of the multiples arise due to chance associations along the line of sight, rather than physically associated systems. The fraction of SCUBA-2 sources with multiple ALMA-detected counterparts in AS2COSMOS is 34 ± 2 per cent, which is significantly higher than the prediction of our simulation. Taken together, these results indicate that ∼30 per cent of the AS2COSMOS multiple maps contain SMGs that are physically associated, a rate that is in good agreement with prior studies of a handful of spectroscopically identified pairs (Hayward et al. 2018; Wardlow et al. 2018) or statistical analysis using photometric redshifts (e.g. Stach et al. 2018).

Finally, we consider whether the fraction of multiples that are physically associated is correlated with the flux density of the secondary SMGs. In Fig. 7, we show the 870-μm flux density distribution of the 76 secondary AS2COSMOS SMGs that are detected within the primary beam of the AS2COSMOS maps. We find that number of secondary sources rises slowly with flux above our limit of $S_{870\,\mu\mathrm{m}} = 6.2$ mJy. Fig. 7 also shows the expected flux distribution of these secondary components, as estimated from our end-to-end simulations of the A/S2COSMOS simulation. As can be seen in Fig. 7, the observed population of secondary AS2COSMOS SMGs with fluxes $\leq$3 mJy is broadly consistent with the results of the simulation; The AS2COSMOS sample contains 41 secondaries with fluxes densities of $S_{870\,\mu\mathrm{m}} = 1$–3 mJy, which agrees precisely with the expected rate of 41 sources from the simulation. However, when we consider secondary sources brighter than $S_{870\,\mu\mathrm{m}} = 3$ mJy, we find clear evidence of an excess of secondary SMGs in AS2COSMOS relative to the simulation. There are 35 AS2COSMOS secondary SMGs at $S_{870\,\mu\mathrm{m}} > 3$ mJy and we estimate that this is a factor of $2.6 \pm 0.5\times$ higher than that expected from an unclustered population.

Any multiplicity in our end-to-end simulation of the AS2COSMOS pilot survey arises due to line-of-sight projections with the primary SMG in each simulated ALMA map. As such, our results indicate that the observed population of 'faint' AS2COSMOS secondaries ($S_{870\,\mu\mathrm{m}} < 3$ mJy) is overwhelmingly dominated by sources seen in projection along the line of sight to the primary SMG in each ALMA map. However, where an AS2COSMOS secondary is detected with a flux density of $S_{870\,\mu\mathrm{m}} > 3$ mJy we estimate that there is a 62 ± 7 per cent chance that it is physically associated with the brightest SMG in the map, a significantly higher rate of association than we estimated for the overall sample (∼30 per cent). Unfortunately, current observational constraints on the relative mix of projected and associated companions in blended SMG maps are weak and so cannot yet provide a conclusive test of these estimates (e.g. Hayward et al. 2018; Stach et al. 2018; Wardlow et al. 2018). Nevertheless, we have a serendipitous detection of an example of one of these physically associated $S_{870\,\mu\mathrm{m}} \gtrsim 3$ mJy secondary SMGs that we discuss next.

3.4 AS2COS 0001.1 and 0001.2

The ALMA observations of the S2COSMOS sample were intended to yield detections of the continuum dust emission from these sources. However, the data are also sensitive to any line emission that serendipitously falls within the available 7.5-GHz bandwidth (e.g. Swinbank et al. 2012). As described by Mitsuhashi et al. (2020), we searched the ALMA data cubes for strong emission lines at the position of each AS2COSMOS source and identified bright line emission from five sources, including both counterparts to the bright SCUBA-2 source S2COSMOS 0001[4]: AS2COS 0001.1 and 0001.2, which we discuss in more detail here. We note that these sources have also been discussed in a very recent paper by Jiménez-Andrade et al. (2020), where they are named AzTEC2-A and AzTEC2-B, respectively, and we compare our results to those from their analysis in the following. We note that the ∼2 per cent detection rate of line emitters in the AS2COSMOS data cubes is comparable to that found in previous SMG studies (Swinbank et al. 2012; Cooke et al. 2018). A detailed discussion of all potential line emitters in the AS2COSMOS pilot survey is presented in Mitsuhashi et al. (2020).

AS2COS 0001.1 and 0001.2 were identified in an archival ALMA observation of S2COSMOS 0001, the highest significance source in the S2COSMOS survey (SNR = 28, $S_{850\,\mu\mathrm{m}} = 16.8$ mJy). The ALMA-detected SMGs have 870-μm flux densities of 13.5 ± 0.3 and 3.6 ± 0.2 mJy – where these fluxes are based on the line-free continuum in the ALMA cubes. As discussed by Mitsuhashi et al. (2020) and Jiménez-Andrade et al. (2020), the ALMA observations of both these sources show significant emission line detections at ∼337 GHz (see Fig. 8).

The $^2\mathrm{P}_{3/2} \rightarrow {}^2\mathrm{P}_{1/2}$ fine structure line of single-ionized atomic carbon (C^+) at 157.7 μm, hereafter [C II], is typically the strongest far-infrared emission line in the spectra of star-forming galaxies (e.g. Brauher, Dale & Helou 2008; Díaz-Santos et al. 2013). The [C II] emission can comprise two per cent of the total bolometric luminosity of a source, and is typically an order of magnitude brighter than other atomic or molecular emission (e.g. [N II] 122 μm, [O I] 145 μm, [N II] 205 μm, or mid-J ^{12}CO). At the depth of our observations, [C II] is the most likely identification for the line emission from AS2COS 0001.1 and 0001.2, placing these sources at a redshift of $z = 4.624 \pm 0.001$ and 4.635 ± 0.001, respectively. This identification has been unambiguously confirmed by the observations of ^{12}CO(5–4) emission in these sources by Jiménez-Andrade et al. (2020) and our redshift measurements agree within the errors with those from Jiménez-Andrade et al. (2020). These two SMGs lie near to a foreground $z = 0.34$ galaxy (see Fig. 4), which results in amplifications of $\mu_{1.1} \sim 1.5$ and $\mu_{1.2} \sim 1.35$ as estimated by Jiménez-Andrade et al. (2020). We have not corrected for this amplification in the following.

To extract kinematic information from the [C II] line emission from AS2COS 0001.1 and 0001.2, we first experimented with applying various tapers to the *uv*-data. We found that tapering the data cube to a synthesized beam of 0.4 arcsec FWHM provided a good comprise between resolution and surface brightness sensitivity to the line emission. Adopting this tapering strategy, we constructed a 'dirty' cube for the field that we cleaned following the same procedure used for the AS2COSMOS continuum maps (see Section 2.2). The cleaned cube reaches a median sensitivity of 1.0 mJy beam^{-1} per 32-MHz channel, and we detect line emission from AS2COS 0001.1 and 0001.2 at an integrated SNR of 32 and 20, respectively (see Fig. 8).

In Fig. 8, we show two-dimensional maps of the intensity and kinematics of the [C II] emission in both SMGs. The kinematic maps were derived from Gaussian fits to the line emission from each source using an adaptive pixel grid; we first consider a single spaxel but, where necessary, adaptively bin pixels to a maximum of 1.5 × beam FWHM until we achieve an SNR > 5 integrated across the line emission. For both AS2COS 0001.1 and 0001.2, we see a clear velocity gradient and centrally peaked velocity dispersion that is indicative of bulk, ordered rotation in the line-emitting gas [in

[4]Also known as AzTEC 2 (Scott et al. 2008).

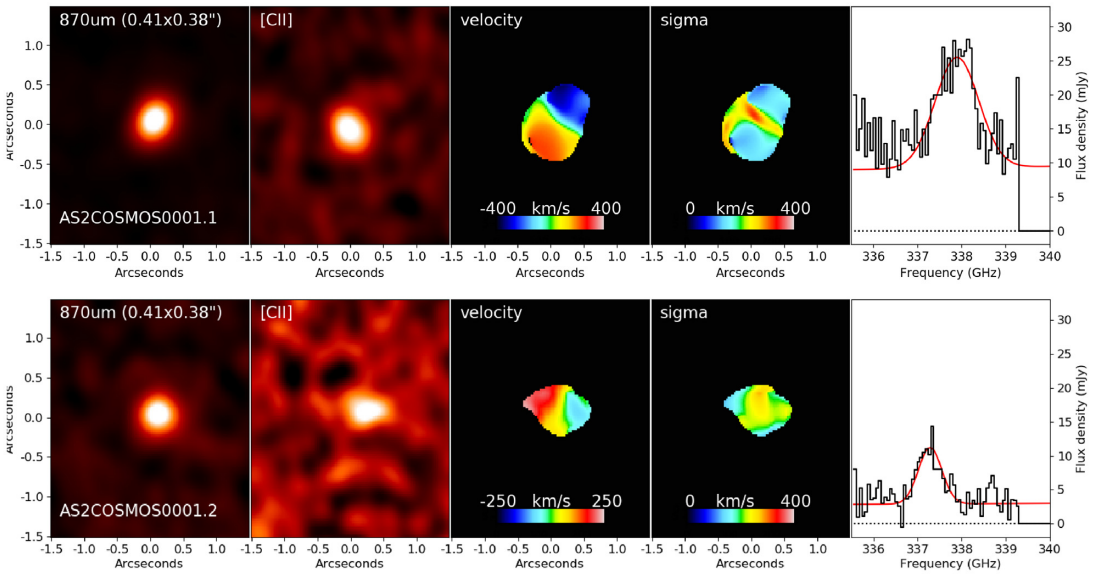

Figure 8. Spatially resolved dust and line emission from AS2COS 0001.1 and 0001.2. From left-to-right: (1) observed 870-μm continuum dust emission; (2) observed, continuum-subtracted [C II] line emission; (3) velocity profile derived from the [C II] kinematics and (4) velocity dispersion, as estimated from the best-fitting Gaussian model to the emission in each spaxel; (5) the spatially integrated [C II] spectrum for each source, along with a Gaussian fit to the lines (the gap between the two pairs of basebands means that there are no data above ∼339.2 GHz). The redshifts derived from the [C II] emission for the two SMGs are $z = 4.624$ and 4.635. We find that the kinematics of both sources show evidence for a clear velocity gradient and a centrally concentrated velocity dispersion, indicative of disc-like rotation in the [C II]-emitting gas. The sources have an on-sky separation of 3.1 arcsec (∼20 kpc) and velocity separation of $590 \pm 40\,\mathrm{km\,s^{-1}}$, suggesting that they are physically associated within the same dark matter halo.

contrast, the more limited spectral coverage employed in Jiménez-Andrade et al. (2020) meant that they were unable to map the full rotation curve in AS2COS 0001.1].

The redshift offset we derive between the two ALMA sources corresponds to a velocity separation of $590 \pm 40\,\mathrm{km\,s^{-1}}$ [this is marginally higher than the $375 \pm 50\,\mathrm{km\,s^{-1}}$ derived from the combined [C II] and ^{12}CO(5–4) line kinematics by Jiménez-Andrade et al. (2020), but this difference does not affect the following discussion]. The two SMGs have an on-sky separation of 3.1 arcsec that, at their estimated redshift, corresponds to a projected spatial separation of ∼20 kpc (before accounting for lensing). To understand whether these SMGs are physically associated, we require knowledge of the mass of the dark matter haloes. Clustering measurements of the S2COSMOS sources, and other SMG samples, suggest that typical SMGs at $z \sim 2$–3 occupy dark matter haloes of $\sim 10^{13}\,\mathrm{M_\odot}$ (An et al. 2019; see also Wilkinson et al. 2017; Stach et al., in preparation). Following the discussion in Wardlow et al. (2018), we can expect that pairs of test masses in a halo with a NFW profile (Navarro, Frenk & White 1997) of mass $\sim 10^{13}\,\mathrm{M_\odot}$ have typical velocity separations of $\sim 700\,\mathrm{km\,s^{-1}}$ for a projected spatial separation of ∼20 kpc. Hence, the observed spatial and velocity offsets between AS2COS 0001.1 and 0001.2 are consistent with them occupying a dark matter halo with a mass of $\sim 10^{13}\,\mathrm{M_\odot}$, suggesting that it is likely that these SMGs are physically associated within a single dark matter halo (see also the discussion of S2COSMOS 0003 in Wang et al. 2016). Based on the orientation of their velocity fields, these two galaxies appear to be co-rotating in a prograde orbit, with a velocity offset comparable to their internal rotation velocities, suggesting the possibility that we are witnessing a rapid and highly efficient merger. This is consistent with the link proposed by Dudzevičiūtė et al. (2020) between the SMG population and the highly efficient collapse of gas-rich massive haloes, with characteristic masses similar to those inferred here.

3.5 Redshift distribution and evolution

We show in Fig. 9 the redshift distribution of the SMGs in our survey derived using the MAGPHYS analysis discussed in Section 2.6 (see also Ikarashi et al., in preparation). This shows the distribution of the median photometric redshift estimated from the PDFs of each source from MAGPHYS, as well as the summed PDFs, which are in good agreement. We determine a median redshift for the full sample of AS2COSMOS SMGs of $z = 2.68 \pm 0.07$, with the subset of sources brighter than our nominal flux limit of $S_{870\,\mu\mathrm{m}} = 6.2$ mJy having a median redshift of $z = 2.87 \pm 0.08$. The latter is marginally higher than the median of $z = 2.61 \pm 0.08$ reported for the somewhat fainter sample of SMGs from AS2UDS by Dudzevičiūtė et al. (2020). Moreover, we note that the AS2COSMOS distribution has a more extended tail to higher redshifts than is seen in the AS2UDS sample, with 10 ± 2 per cent of AS2COSMOS sources located at $z_{\mathrm{phot}} \geq 4$ (and 13 ± 3 per cent of those brighter than $S_{870\,\mu\mathrm{m}} = 6.2$ mJy) compared to ∼6 per cent in AS2UDS.

Focusing on just the brightest SMGs, we estimate a median redshift of $z = 3.24 \pm 0.19$ for the 20 AS2COSMOS SMGs with 870-μm fluxes above 12 mJy, which is also marginally higher than the median of $z = 2.79 \pm 0.05$ for the 364 SMGs in AS2UDS brighter than the 3.6 mJy single-dish flux limit of that study (Dudzevičiūtė et al. 2020). In addition, we can also construct a sample of faint SMGs using the 14 SMGs with $S_{870\,\mu\mathrm{m}} \leq 1$ mJy in the combined AS2COSMOS and AS2UDS samples, which have a median redshift of just $z = 2.44 \pm 0.34$ (although we

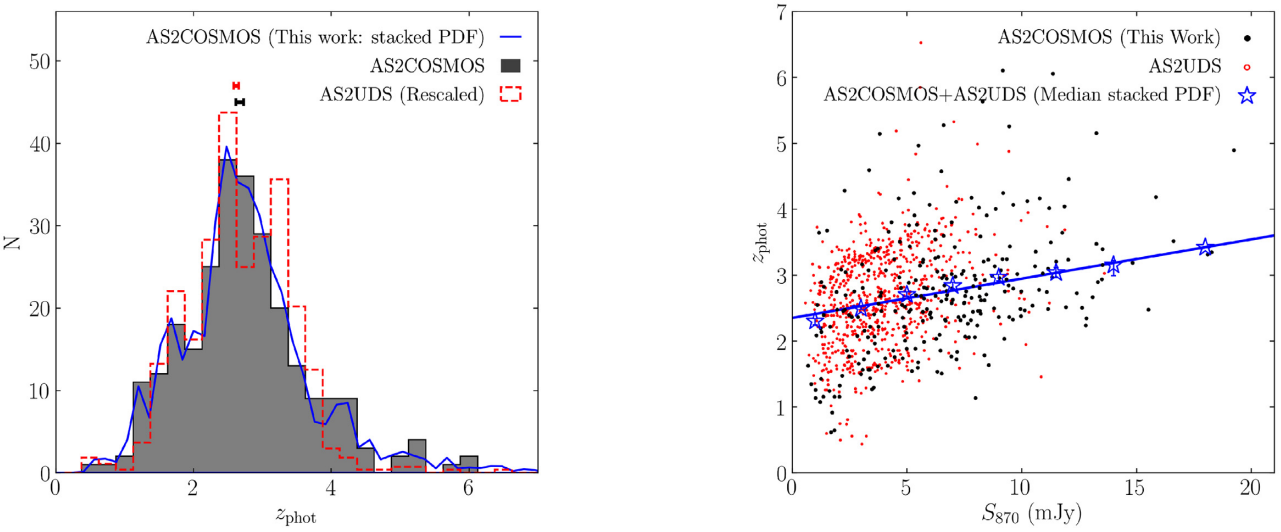

Figure 9. *Left:* The photometric redshift distribution of the AS2COSMOS SMGs, as determined from our MAGPHYS analysis of their ultraviolet-to-radio spectral energy distributions. For a comparison, we show the redshift distribution for the AS2UDS sample, normalized to match the AS2COSMOS sample size. The AS2COSMOS sample has a median photometric redshift of $z_{\rm phot} = 2.68 \pm 0.06$, which is broadly comparable to the median of $z_{\rm phot} = 2.61 \pm 0.04$ determined for AS2UDS. However, we note that the AS2COSMOS distribution has a more extended tail to higher redshifts than is seen in the AS2UDS sample, with 10 ± 2 per cent of AS2COSMOS sources located at $z_{\rm phot} \geq 4$ (and 13 ± 3 per cent of those brighter than $S_{870\,\mu\rm m} = 6.2$ mJy) compared to $\sim$6 per cent in AS2UDS. The stacked, normalized probability distribution function for all AS2COSMOS sources is shown and is comparable to the median redshift distribution, indicating that our results are not sensitive to asymmetries in the redshift solutions for individual SMGs. *Right:* The median photometric redshift of the AS2COSMOS and AS2UDS sources, as a function of their 870-μm flux densities. We identify a clear trend of increasing redshift with 870-μm flux density, in agreement with results from the AS2UDS survey (Stach et al. 2018). We bin the combined AS2COSMOS and AS2UDS surveys by 870-μm flux density and show the median of the stacked PDF for all sources in each bin. A linear fit to the median in each bin yields a gradient of 0.06 ± 0.01, indicating strong evolution in the average flux density of the SMG population with redshift.

caution that around half of these are secondary components in the maps of brighter SMGs and so may not represent an unbiased population, but see the discussion of faint secondary SMGs in Section 3.3).

The comparison of the median redshifts with sub-millimetre flux of the various samples suggests a trend and so to better constrain the variation in the redshift with $S_{870\,\mu\rm m}$ we also show in Fig. 9 the distribution for the combined AS2COSMOS and AS2UDS samples. Stach et al. (2019) reported a trend between $S_{870\,\mu\rm m}$ and redshift in the AS2UDS survey, following earlier suggestions going back over more than two decades (Archibald et al. 2001; Ivison et al. 2002, 2007). By employing the wider area and typically brighter AS2COSMOS sample, we can extend the flux range available to assess this trend. Indeed, Fig. 9 shows a strong trend of increasing 870-μm flux with redshift for the combined sample. We measure a gradient of the trend in redshift with 870-μm flux of 0.06 ± 0.01 mJy^{-1} for the combined sample, compared to 0.09 ± 0.02 mJy^{-1} estimated from just the AS2UDS survey by Stach et al. (2019). This trend between observed 870-μm flux density and redshift is most likely driven by the increasing gas fraction in these systems and hence gas (and dust) mass in more distant galaxies, compounded by the growing far-infrared luminosities driven by the higher SFRs, which are fuelled in turn by these more extensive reservoirs of gas (Dudzevičiūtė et al. 2020; Ikarashi et al., in preparation).

4 CONCLUSIONS

We have presented the results of an ALMA 870-μm continuum survey of the brightest sub-millimetre sources drawn from the SCUBA-2 survey of the COSMOS field (S2COSMOS; Simpson et al. 2019; An et al. 2019). Using a combination of our pilot study of 158 SCUBA-2 sources and comparable observations of a further 24, we construct an effectively complete sample (182/183) of the sources with inferred 850-μm flux densities of $\geq$6.2 mJy from the S2COSMOS survey of the 1.6-deg^2 COSMOS field. The ALMA maps detect 260 SMGs with flux densities of $S_{870\,\mu\rm m} = 0.7$–19.2 mJy across the 182 fields. The main conclusions of this study are as follows:

(i) We detect multiple SMGs in 34 ± 2 per cent of SCUBA-2 sources, or 53 ± 8 per cent for sources brighter than $S_{850\,\mu\rm m} > 12$ mJy, underlining the fact that blending of more than one SMG is a significant issue for single-dish surveys. We estimate that approximately one-third of these SMG–SMG pairs are physically associated; predominantly, these are the brighter secondary systems with $S_{870\,\mu\rm m} \gtrsim 3$ mJy. We illustrate these associated systems using the serendipitous detection of bright [C II] 157.74-μm line emission in the ALMA observations of two SMGs associated with the highest signal-to-noise SCUBA-2 source in the field: AS2COS 0001.1 and 0001.2 at $z = 4.63$.

(ii) We show that the number counts derived from our ALMA observations lie below the raw counts of sources in the S2COSMOS SCUBA-2 survey, but after applying an end-to-end modelling approach, which accounts for both source blending and noise boosting (Simpson et al. 2019), the corrected counts from the single-dish survey are in good agreement with those determined from our ALMA observations. We use this survey and the comparable AS2UDS study of an $\sim$1-deg^2 field to derive rough bounds on the

contribution of cosmic variance to the number counts and show that these are consistent with predictions from theoretical models.

(iii) We construct the multiwavelength SED of the AS2COSMOS SMGs using the extensive archival data of this field and model these with MAGPHYS to estimate their photometric redshifts. We find a median photometric redshift for the $S_{850\,\mu m} > 6.2$ mJy AS2COSMOS sample of $z = 2.87 \pm 0.08$, and clear evidence for evolution in the median redshift with 870-μm flux density suggesting strong evolution in the bright end of the 870-μm luminosity function. This is most likely driven by the increasing gas fractions and concomitant high SFRs, and hence dust masses in more distant galaxies (Ikarashi et al., in preparation).

ACKNOWLEDGEMENTS

We thank the Referee and Editor for comments that have improved the clarity and presentation of this work. The Durham co-authors acknowledge support from STFC (ST/P000541/1 and ST/T000244/1) and JMS gratefully acknowledges support from the EACOA fellowship programme. UD and JEB acknowledge the support of STFC studentships (ST/R504725/1 and ST/S50536/1, respectively). YM acknowledges JSPS KAKENHI grant nos. 25287043, 17H04831, and 17KK0098. WHW acknowledges grant support from the Ministry of Science and Technology of Taiwan (105-2112-M-001-029-MY3 and 108-2112-M-001-014-MY3). YA acknowledges financial support through NSFC grant 11933011. KEKC acknowledges support from STFC (ST/R000905/1) and a Royal Society/Leverhulme Trust Senior Fellowship (SRF/R1/191013). This paper makes use of the following ALMA data: ADS/JAO.ALMA#2016.1.00463.S. ALMA is a partnership of ESO (representing its member states), NSF (USA), and NINS (Japan), together with NRC (Canada), NSC and ASIAA (Taiwan), and KASI (Republic of Korea), in cooperation with the Republic of Chile. The Joint ALMA Observatory is operated by ESO, AUI/NRAO, and NAOJ. This analysis used data from the S2COSMOS survey (M16AL002) on the JCMT, which in turn included data from S2CLS (MJLSC02) and the JCMT archive. The JCMT is operated by the East Asian Observatory on behalf of The National Astronomical Observatory of Japan; Academia Sinica Institute of Astronomy and Astrophysics; the Korea Astronomy and Space Science Institute; the Operation, Maintenance and Upgrading Fund for Astronomical Telescopes and Facility Instruments, budgeted from the Ministry of Finance (MOF) of China and administrated by the Chinese Academy of Sciences (CAS); and the National Key R&D Program of China (No. 2017YFA0402700). Additional funding support is provided by the Science and Technology Facilities Council of the United Kingdom and participating universities in the United Kingdom and Canada (ST/M007634/1, ST/M003019/1, and ST/N005856/1). The JCMT has historically been operated by the Joint Astronomy Centre on behalf of the Science and Technology Facilities Council of the United Kingdom, the National Research Council of Canada, and the Netherlands Organization for Scientific Research and data from observations undertaken during this period of operation are used in this manuscript. This research used the facilities of the Canadian Astronomy Data Centre operated by the National Research Council of Canada with the support of the Canadian Space Agency.

REFERENCES

Aihara H. et al., 2019, PASJ, 71, 114
An F. X. et al., 2019, ApJ, 886, 48
Aravena M., Younger J. D., Fazio G. G., Gurwell M., Espada D., Bertoldi F., Capak P., Wilner D., 2010, ApJ, 719, L15
Archibald E. N., Dunlop J. S., Hughes D. H., Rawlings S., Eales S. A., Ivison R. J., 2001, MNRAS, 323, 417
Barger A. J. et al., 2014, ApJ, 784, 9
Battisti A. J. et al., 2019, ApJ, 882, 61
Baugh C. M., Lacey C. G., Frenk C. S., Granato G. L., Silva L., Bressan A., Benson A. J., Cole S., 2005, MNRAS, 356, 1191
Berta S. et al., 2011, A&A, 532, A49
Bertin E., Arnouts S., 1996, A&AS, 117, 393
Biggs A. D., Ivison R. J., 2008, MNRAS, 385, 893
Blain A. W., Chapman S. C., Smail I., Ivison R., 2004, ApJ, 611, 725
Bothwell M. S. et al., 2013, MNRAS, 429, 3047
Brauher J. R., Dale D. A., Helou G., 2008, ApJS, 178, 280
Brisbin D. et al., 2017, A&A, 608, A15
Brusa M. et al., 2010, ApJ, 716, 348
Bussmann R. S. et al., 2015, ApJ, 812, 43
Casey C. M., 2016, ApJ, 824, 36
Chabrier G., 2003, PASP, 115, 763
Chakrabarti S., Fenner Y., Cox T. J., Hernquist L., Whitney B. A., 2008, ApJ, 688, 972
Chapman S. C., Blain A. W., Smail I., Ivison R. J., 2005, ApJ, 622, 772
Chen C.-C. et al., 2015, ApJ, 799, 194
Chen C.-C. et al., 2016, ApJ, 820, 82
Civano F. et al., 2016, ApJ, 819, 62
Cooke E. A. et al., 2018, ApJ, 861, 100
Cowie L. L., González-López J., Barger A. J., Bauer F. E., Hsu L. Y., Wang W. H., 2018, ApJ, 865, 106
Cowley W. I., Lacey C. G., Baugh C. M., Cole S., 2015, MNRAS, 446, 1784
da Cunha E., Charlot S., Elbaz D., 2008, MNRAS, 388, 1595
da Cunha E. et al., 2015, ApJ, 806, 110
Dannerbauer H. et al., 2014, A&A, 570, A55
Davé R., Finlator K., Oppenheimer B. D., Fardal M., Katz N., Kereš D., Weinberg D. H., 2010, MNRAS, 404, 1355
Dempsey J. T. et al., 2013, MNRAS, 430, 2534
Díaz-Santos T. et al., 2013, ApJ, 774, 68
Dudzevičiūtė U. et al., 2020, MNRAS, 494, 3828
Dunlop J. S. et al., 2017, MNRAS, 466, 861
Eddington A. S., 1913, MNRAS, 73, 359
Fazio G. G. et al., 2004, ApJS, 154, 10
Franco M. et al., 2018, A&A, 620, A152
Geach J. E. et al., 2017, MNRAS, 465, 1789
Gehrels N., 1986, ApJ, 303, 336
Griffin M. J. et al., 2010, A&A, 518, L3
Gullberg B. et al., 2019, MNRAS, 490, 4956
Harikane Y. et al., 2019, ApJ, 883, 142
Harrington K. C. et al., 2016, MNRAS, 458, 4383
Hatsukade B. et al., 2018, PASJ, 70, 105
Hayward C. C. et al., 2018, MNRAS, 476, 2278
Hickox R. C. et al., 2009, ApJ, 696, 891
Hill R. et al., 2018, MNRAS, 477, 2042
Hodge J. A. et al., 2016, ApJ, 833, 103
Holland W. S. et al., 2013, MNRAS, 430, 2513
Hsieh B.-C., Wang W.-H., Hsieh C.-C., Lin L., Yan H., Lim J., Ho P. T. P., 2012, ApJS, 203, 23
Ikarashi S. et al., 2011, MNRAS, 415, 3081
Ikarashi S. et al., 2015, ApJ, 810, 133
Ivison R. J. et al., 2002, MNRAS, 337, 1
Ivison R. J. et al., 2007, MNRAS, 380, 199
Ivison R. J., Smail I., Papadopoulos P. P., Wold I., Richard J., Swinbank A. M., Kneib J.-P., Owen F. N., 2010, MNRAS, 404, 198
Ivison R. J. et al., 2013, ApJ, 772, 137
Jiménez-Andrade E. F. et al., 2020, ApJ, 890, 171
Jin S. et al., 2018, ApJ, 864, 56
Karim A. et al., 2013, MNRAS, 432, 2
Koekemoer A. M. et al., 2007, ApJS, 172, 196
Lacey C. G. et al., 2016, MNRAS, 462, 3854

Laigle C. et al., 2016, ApJS, 224, 24
Le Floc'h E. et al., 2009, ApJ, 703, 222
Lilly S. J., Eales S. A., Gear W. K. P., Hammer F., Le Fèvre O., Crampton D., Bond J. R., Dunne L., 1999, ApJ, 518, 641
Liu D. et al., 2018, ApJ, 853, 172
Liu D. et al., 2019, ApJ, 887, 235
Lutz D. et al., 2011, A&A, 532, A90
McAlpine S. et al., 2019, MNRAS, 488, 2440
McCracken H. J. et al., 2012, A&A, 544, A156
Magnelli B. et al., 2013, A&A, 553, A132
Miettinen O. et al., 2015, A&A, 584, A32
Mitsuhashi I. et al., 2020, ApJ, in press
Navarro J. F., Frenk C. S., White S. D. M., 1997, ApJ, 490, 493
Oliver S. J. et al., 2012, MNRAS, 424, 1614
Oteo I., Zwaan M. A., Ivison R. J., Smail I., Biggs A. D., 2016, ApJ, 822, 36
Poglitsch A. et al., 2010, A&A, 518, L2
Robotham A. S. G., Taranu D. S., Tobar R., Moffett A., Driver S. P., 2017, MNRAS, 466, 1513
Rowan-Robinson M., 2000, MNRAS, 316, 885
Rowan-Robinson M., Wang L., 2010, MNRAS, 406, 720
Sanders D. B. et al., 2007, ApJS, 172, 86
Scott K. S. et al., 2008, MNRAS, 385, 2225
Scott K. S. et al., 2012, MNRAS, 423, 575
Simpson J. M. et al., 2014, ApJ, 788, 125
Simpson J. M. et al., 2015a, ApJ, 799, 81
Simpson J. M. et al., 2015b, ApJ, 807, 128
Simpson J. M. et al., 2019, ApJ, 880, 43
Smolčić V. et al., 2012, A&A, 548, A4
Smolčić V. et al., 2017, A&A, 602, A1
Stach S. M. et al., 2018, ApJ, 860, 161
Stach S. M. et al., 2019, MNRAS, 487, 4648
Steinhardt C. L. et al., 2014, ApJ, 791, L25
Strandet M. L. et al., 2016, ApJ, 822, 80
Swinbank A. M., Chapman S. C., Smail I., Lindner C., Borys C., Blain A. W., Ivison R. J., Lewis G. F., 2006, MNRAS, 371, 465
Swinbank A. M. et al., 2008, MNRAS, 391, 420
Swinbank A. M. et al., 2010a, MNRAS, 405, 234
Swinbank A. M. et al., 2010b, Nature, 464, 733
Swinbank A. M. et al., 2012, MNRAS, 427, 1066
Swinbank A. M. et al., 2014, MNRAS, 438, 1267
Tacconi L. J. et al., 2008, ApJ, 680, 246
Tazzari M., Beaujean F., Testi L., 2018, MNRAS, 476, 4527
Thomson A. P. et al., 2019, ApJ, 883, 204
Wang T. et al., 2016, ApJ, 828, 56
Wang W.-H., Cowie L. L., van Saders J., Barger A. J., Williams J. P., 2007, ApJ, 670, L89
Wang W.-H., Cowie L. L., Barger A. J., Williams J. P., 2011, ApJ, 726, L18
Wardlow J. L. et al., 2018, MNRAS, 479, 3879
Wilkinson A. et al., 2017, MNRAS, 464, 1380
Younger J. D. et al., 2007, ApJ, 671, 1531
Younger J. D. et al., 2009, ApJ, 704, 803

SUPPORTING INFORMATION

Supplementary data are available at *MNRAS* online.

Table 1. AS2COSMOS source catalogue.

Please note: Oxford University Press is not responsible for the content or functionality of any supporting materials supplied by the authors. Any queries (other than missing material) should be directed to the corresponding author for the article.

APPENDIX A

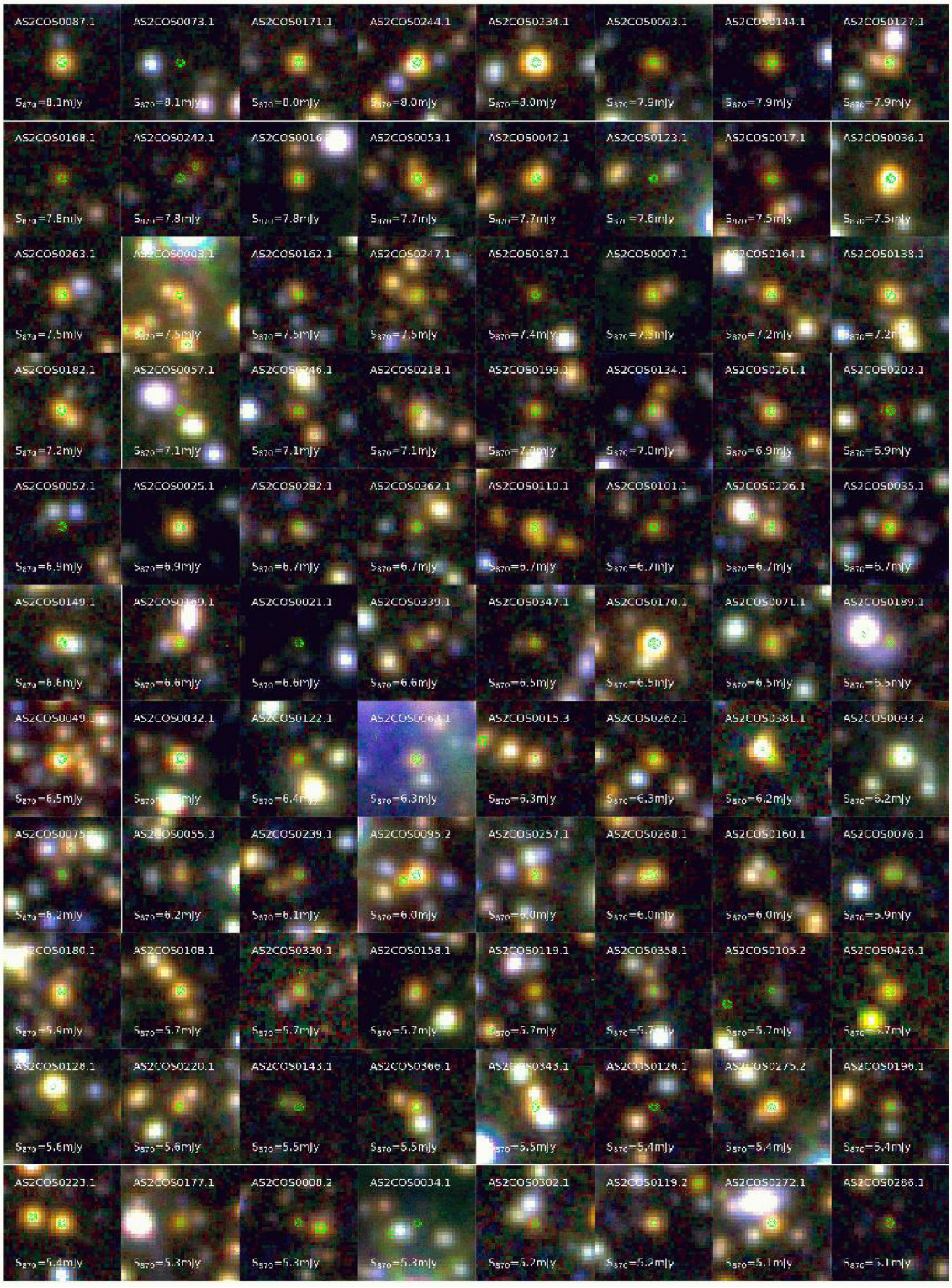

Figure A1. 20 arcsec × 20 arcsec images showing the K_s, 3.6- and 4.5-μm (corresponding to BGR channels) colour images of the faintest 180/260 ASCOSMOS SMGs, those with $S_{870\,\mu m} \leq 8.5$ mJy. Each of the images is centred on the ALMA source position and are ordered by decreasing ALMA 870-μm flux density. Contours represent that the ALMA 870-μm detections are overlaid at 4σ, 10σ, 20σ, and 50σ. Along with the brighter SMGs shown in Fig. 4, these images demonstrate that the AS2COSMOS SMGs are typically very red and/or faint at near-to-mid-infrared wavelengths, relative to the field population. We note that the apparent frequency of ALMA-detected companions in the fields of the fainter sources is simply a result of these sources being so faint that they are only included in our sample if they lie in close proximity to a brighter SMG.

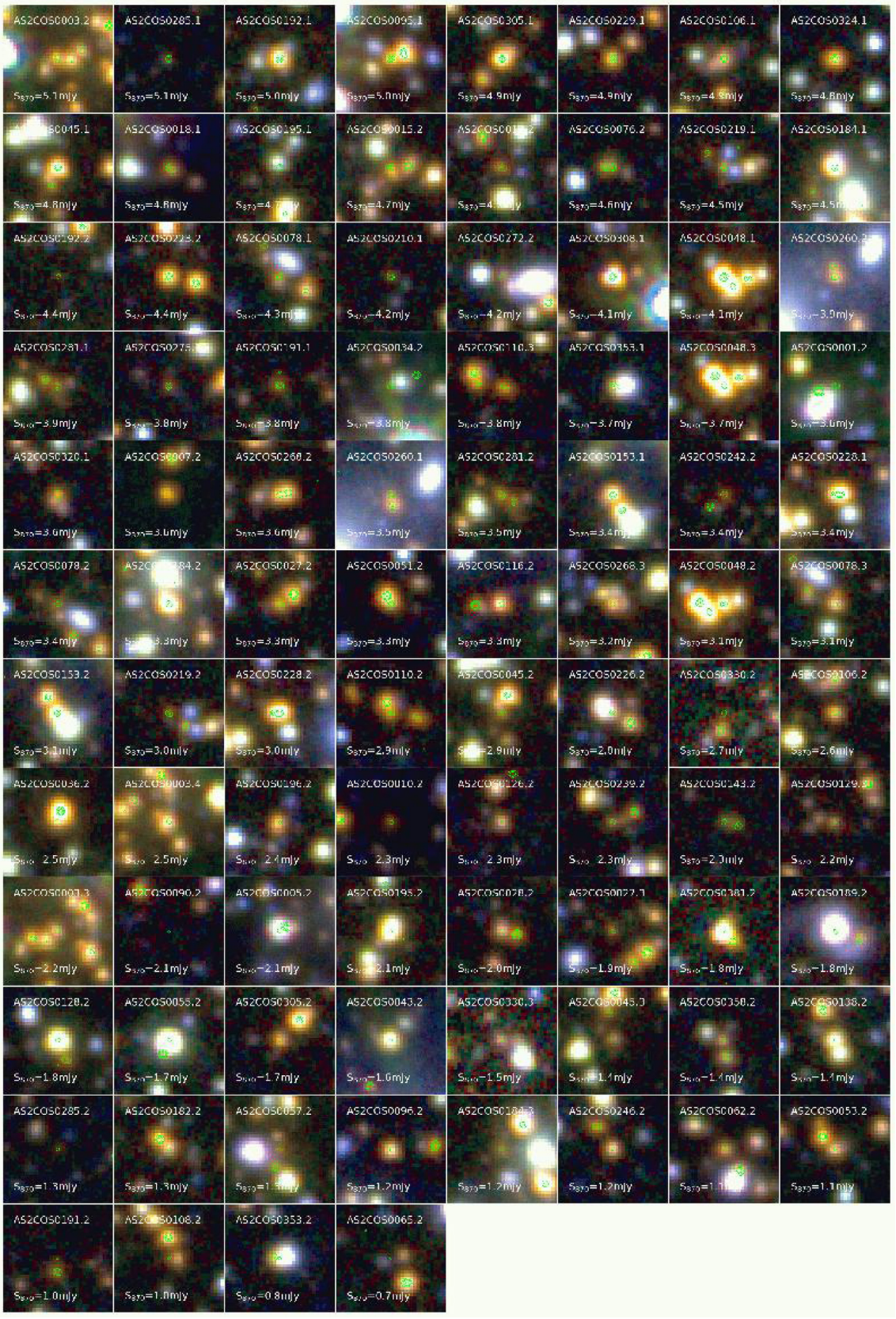

Figure A1 – *continued*

[1]*Centre for Extragalactic Astronomy, Department of Physics, Durham University, South Road, Durham DH1 3LE, UK*
[2]*Academia Sinica Institute of Astronomy and Astrophysics, No. 1, Section 4, Roosevelt Rd., Taipei 10617, Taiwan*
[3]*National Astronomical Observatory of Japan, 2-21-1 Osawa, Mitaka, Tokyo 181-8588, Japan*
[4]*The Graduate University for Advanced Studies (SOKENDAI), Osawa, Mitaka, Tokyo 181-8588, Japan*
[5]*Inter-University Institute for Data Intensive Astronomy, and Department of Physics and Astronomy, University of the Western Cape, Robert Sobukwe Road, Bellville 7535, Cape Town, South Africa*
[6]*Purple Mountain Observatory, Chinese Academy of Sciences, Nanjing 210033, Jiangsu, People's Republic of China*
[7]*School of Astronomy and Space Science, University of Science and Technology of China, Hefei 230026, Anhui, People's Republic of China*
[8]*Department of Physics, University of Oxford, Keble Road, Oxford OX1 3RH, UK*
[9]*Department of Physics and Astronomy, University of British Columbia, 6225 Agricultural Road, Vancouver, BC V6T 1Z1, Canada*
[10]*National Research Council, Herzberg Astronomy and Astrophysics, 5071 West Saanich Road, Victoria, BC V9E 2E7, Canada*
[11]*Department of Physics and Atmospheric Science, Dalhousie University, Halifax, NS B3H 4R2, Canada*
[12]*Centre for Astrophysics Research, School of Physics, Astronomy and Mathematics, University of Hertfordshire, College Lane, Hatfield AL10 9AB, UK*
[13]*European Southern Observatory, Karl Schwarzschild Strasse 2, D-85748 Garching, Germany*
[14]*Institute of Astronomy, School of Science, The University of Tokyo, 2-21-1 Osawa, Mitaka, Tokyo 181-0015, Japan*
[15]*Nishi-Harima Astronomical Observatory, Centre for Astronomy, University of Hyogo 407-2 Nishigaichi, Sayo, Sayo-gun, Hyogo 679-5313, Japan*
[16]*RIKEN Cluster for Pioneering Research, 2-1 Hirosawa, Wako-shi, Saitama 351-0198, Japan*
[17]*Kavli Institute for Astronomy and Astrophysics, Peking University, Haidian District, Beijing 100871, People's Republic of China*
[18]*Yunnan Observatories, Chinese Academy of Sciences, Guandu District, Kunming 650011, People's Republic of China*

This paper has been typeset from a TEX/LATEX file prepared by the author.